Necessary corrections of the mathematical foundation of fracture mechanics

- the incompatibility of the applied boundary value analysis solution of linear elastic fracture mechanics
- the incorrect shear stress transformation – the incorrect field stress extrapolation; - the absence of the "mixed mode" fracture criterion as necessary result of the boundary value problem solution; - the absence of the determining strain rate behavior according to molecular deformation kinetics, and the absence of Limit analysis approach for correction and replacement of so called nonlinear fracture mechanics, which wrongly is based on a not existent critical energy release rate for each stress type, based on the elastic energy release crack opening modes.

T.A.C.M. van der Put,
TU-Delft, Civil Engineering and Geosciences, Wood Science c/o Section Biobased Structures and Materials
c/o Wielengahof 16 NL2625 LJ Delft, The Netherlands
corresponding author, Tel: +31 152851980, E-mail: vanderp@xs4all.nl

Keywords: Fracture mechanics; Notch fracture boundary value analysis; fracture limit analysis; isotropic and orthotropic materials with isotropic matrix like wood

Abstract

It is shown, that the applied fracture mechanics textbook crack tip boundary value problem solution is identical to the sum of the exact solutions of pure normal stress loading alone, and of pure shear stress loading alone, although these two solutions exclude each other and cannot apply at the same time. Evidently this is against the existing "mixed mode" failure criterion in all acting stresses, which necessarily follows as exact solution of the crack boundary value problem. Further, the applied equations apply for lower order distances to the crack tip singularity (2?? orders lower than the crack length) but are wrongly applied to any distance up to infinity). By an improper small variables transformation, the pure shear crack tip boundary value solution is shown to be not correct. This all delivers, a wrong, incompatible, equilibrium system, which does not show possible displacements and does not satisfy the crack boundary conditions and failure criterion, thus does not represent linear elastic fracture mechanics. As correction, the right exact limit analysis solution is given, which, as such, provides the derivation of the "mixed I-II-mode" fracture criterion, which is precisely verified by empirical research. It further is shown that the postulated textbook stress function is based on integration of the copied mono-mode stress solutions, without regarding right crack-boundary values. The copied mono-mode stress solutions, are shown to be based on the Stevenson potentials for flat elliptical cracks. The necessary limit analysis approach for failure, as exact calculation method, provides the necessary linear elastic analysis up to yield. Linear elastic stress and displacement terms also represent the none vanishing first order row expansion terms of virtual work behavior, of any non-linear stress division. This

has consequences for assumed non-linear elastic fracture mechanics, which is shown, to be replaceable by the linear approach of limit analysis. As example, the critical stress intensity is given of a test series with different initial crack lengths, which, in terms of nonlinear fracture mechanics, was subject to undeterminable critical *J*-integral behavior.

1. Introduction

For a rigorous strength calculation approach, it is necessary to apply limit analysis, which is based on virtual work theorems. For a lower bound solution, it then is possible to regard linear elastic unloading and reloading behavior up to the failure state. It is shown, that the exact boundary value approach leads to a general, mixed mode, fracture criterion, which also is shown to be precisely verified by empirical research (see Table 1). Wood e.g. can be considered to be a reinforced orthotropic polymer. Regarded is also fracture of the isotropic wood matrix, by matrix stresses, up to yield of the reinforcement. Discussed, in the light of limit analysis, are the applicability of the fully empirical critical J-integral- and HRR-method and the necessary replacement of assumed nonlinear elastic behavior, by limit analysis, based e.g. on test results of Bazant (see Fig. 7.1). Comparison is made of the exact solution with the general accepted and prescribed textbook equations, which appear to be based on a transformation to confocal polar coordinates of the exact elliptical coordinate equations which only apply very close to the crack-tip singularity (two?? orders lower than order one) and for shear also only for low order small angles. The proof is given, that these accepted textbook equations of fracture mechanics violate compatibility conditions and the ultimate load criterion, thus don't represent linear elastic fracture mechanics solutions. This is the case because these equations are literal copies of the sum of the exact equations for pure mode I and for pure mode II, which cannot act together at the same time. As correction it is shown that the exact equations, which regard the boundary conditions along the whole crack length, deliver the necessary mixed I-II-mode fracture criterion. It further is shown that lower bound limit analysis solutions are necessary for applicability of theory. Description of an increasing non-linear loading behavior is not needed to estimate behavior at the ultimate state. The needed essential approach of strain- and damage rate equations of molecular deformation kinetics, for a real description of flow and damage behavior, is lacking in textbooks, but is available, in a limit analysis format in the first two references. To make application of this theory possible, it is necessary to leave the inexistent "non-linear elasticity" approach. This also is necessary, because its fundamental starting point of a critical energy release rate

criterion for fracture, is shown to only exist, when it is coupled to a critical stress or critical stress intensity condition.

2. Limit analysis approach of Fracture mechanics

The energy approach of Griffith leads for crack growth, to eq.(2.1):

$$\sigma_g = \sqrt{EG_c / \pi c} \tag{2.1}$$

where σ_g is the critical mode I tensile stress perpendicular to the flat crack; E, the modulus of elasticity; G_c, the critical energy release rate and c, half the crack length.

The same applies for two-dimensional stresses, leading to:

$$\sigma_1^2 \cos^2(\beta) + \sigma_2^2 \sin^2(\beta) = \sigma_y^2 + \tau_{xy}^2 = G_c E / \pi c \tag{2.2}$$

where τ_{xy} is the shear stress along the crack plane. When a determining critical G_c or J-integral J_c, would exist, then eq.(2.2) wrongly predicts, against measurements, that the pure tensile strength (when $\tau_{xy} = 0$) and the pure shear strength (when $\sigma_y = 0$) are equal. This error already was known in the time of Griffith and it was concluded, that, although there is enough energy for failure, the stresses at the failure site have to be high enough for crack extension. An ultimate stress criterion is necessary. A critical energy release rate G_c or J_c, thus is, as such, not a material property and is not able to predict strength. It only exists in an ultimate stress criterion, in all possible acting stresses. Then a compatible critical stress intensity for each acting stress type is known, when acting alone. The applied, so called G-criterion, eq.(2.3), which is eq.(2.2), multiplied by πc, (written as stress intensity factors), is:

$$K_c^2 = K_I^2 + K_{II}^2 \tag{2.3}$$

what is not right as failure criterion:

$$K_c^2 \neq K_I^2 + K_{II}^2 \tag{2.4}$$

because eq.(2.3) predicts an equal tension and shear strength. This thus also applies for the fundamental fracture mechanics equation (2.5) of:

$$G_c = \frac{K_I^2}{E'} + \frac{K_{II}^2}{E'} + \frac{K_{III}^2}{2\mu} \tag{2.5}$$

where $E' = E$ for plane stress, or $E/(1-\upsilon^2)$ for plane strain and μ is the shear modulus. Because of the arbitrary assumed energy addition rule as strength criterion, also K_{III} is simply added by eq.(2.5). To correct for inequal tensile and shear strengths eq.(2.5) is replaced by eq.(2.6).

$$1 = \frac{K_I^2}{K_{Ic}^2} + \frac{K_{II}^2}{K_{IIc}^2} \tag{2.6}$$

which still is mentioned to be a summation of energies, but is an arbitrary empirical equation which, as such, is rejected by the statistical “lack of fit” test, equation 5 of Table 1, as applies for all empirical equations. By eq.(2.2) only the uniaxial strengths of tension alone, or of shear alone, can be obtained. Necessary for compatibility is a general mixed mode stress failure criterion in all possible acting stresses, which, as consequence, determines G_c for each acting stress type alone, when all other stresses are taken to be zero. Application of this mixed mode failure criterion of wood, eq.(4.13), in e.g. [3], did show, for isotropic materials and thus for the isotropic wood matrix (for matrix stresses), that:

$$G_{IIC} = 4G_{IC} \rightarrow K_{IIc} = 2K_{Ic} \tag{2.7}$$

Measurements show that this difference is higher, due to apparent hardening in the shear test and early instability of the tensile test. Fracture of e.g. notched beams did show, that, despite dominant shear loading and the start of local shear flow and shear stress redistribution, (far away from the fracture site), mode I failure was determining, (See [3], Fig.2.4.4). Again, not an energy criterion, thus not an energy release rate or *J*, but a local tensile stress strength criterion, at the crack tip boundary, is determining, what applies the same for any stress combination. Thus, contrary to the general assumption is, G_c (or J_c) in eq.(2.2) or eq.(2.5) not a determining material property.

Because the isotropic wood-matrix is determining for initial fracture, linear elastic fracture mechanics (LEFM) for matrix stresses, applies for initial fracture of wood. Plastic like deformation of the polymeric reinforcement occurs at creases at the crack tip, called fracture process zone. This zone of hydrostatic tension also is the location of micro crack and small crack multiplication and propagation. Macro yield occurs at the highest elastic stress, which occurs at the crack tip boundary, what also is the location of the highest ultimate strain after local yield and thus is the location of crack extension. This zone of confined plasticity behavior also can be replaced by the equivalent linear elastic ultimate stress division. This is similar to the applied linear elastic bending strength diagram of beam theory to represent the elastic- full plastic bending compression stress diagram as given in Fig. 2.1. The difference is an internal equilibrium system, which, as all initial stresses and initial deformations, does not affect the collapse load, according to limit analysis theorems, when original coordinate dimensions are retained in the calculation (as always is applied). Thus Fig. 2.1 shows linear elastic bending with a bending stress σ_m with a negligible internal equilibrium system according to limit analysis. (For profiles, this leads to a profile factor for σ_m). This explains the linear unloading and linear reloading up to yield and explains why LEFM may apply up

to failure by the empirical ultimate uniaxial (tangential) tensile stress at the crack boundary. Thus a, at the start, linear elastic loading curve will bend off by a gradual increasing damage and plasticity (see Fig.2.2). When next, near the top of the loading curve, the specimen is unloaded, this will be a linear elastic unloading line (according to the superposed linear

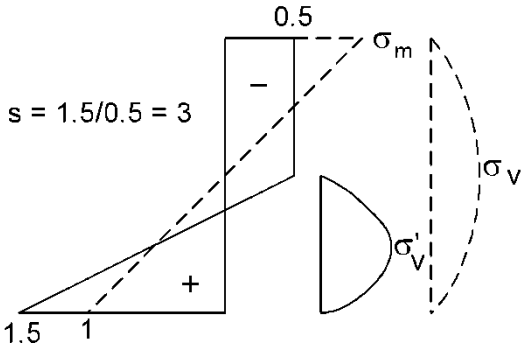

Figure 2.1. Bending stress diagram

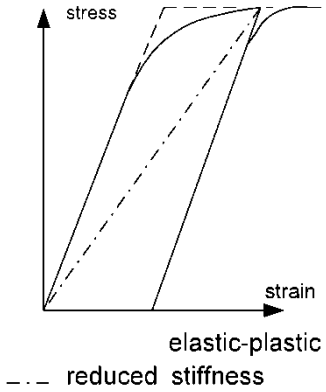

Figure 2.2. Elastic –full plastic behavior

bending stress diagram in Fig. 2.1). When next, reloaded, the curve shows (by the superposed same linear bending stress diagram) linear elastic- full plastic behavior. Thus a linear loading line, up to plastic yield is possible. And, because by plastic flow and damage, the elastic stress is not involved and not changed by that, (according to limit analysis theorems), and thus plays no part in the collapse at limit load, it also is possible to choose a reduced stiffness of the linear elastic loading line, (the dash-dot line of Fig. 2.2) up to flow, as is applied in the Building Codes, based on a chosen total strain. Thus linear behavior up to ultimate state, where the normality rule applies at infinitesimal flow, is the basis of limit analysis, and therefore of the linear elastic boundary value analysis, of fracture mechanics. This is applied in § 4, for the lower bound limit analysis solution. When this solution shows no discontinuity of displacements, it is the unique solution and when the ultimate value is confirmed by precise measurements, (see § 5) which always can be made to represent the lowest upper bound mechanism, the solution also is the exact solution. Fig. 2.2 shows, that possible linear elastic behavior up to failure, is a law of nature. This elementary linear elastic approach up to failure, is the consequence of application of the virtual work approach of limit analysis. To avoid configurational changes, virtual work and virtual displacements should be applied in analyses and thus only first expanded of the load, displacements and stress division apply, because second and higher order quantities are zero in the virtual limit. For that reason design is normally based on the first expanded of a Fourier expansion of the load [4]. For that reason

also, elementary beam theory applies for strength calculations of the Building Codes and for the compliance method of fracture mechanics ([3] § 6.2) to calculate deflection differences. The mean normal stress, the linear bending stress diagram, and parabolic shear stress diagram, are the first expanded of a row expansion of any form of the bending stress diagram. Thus the linear elastic loading behavior represents the accountable first expanded of any non-linear loading behavior and non-linear elastic fracture mechanics can and should be replaced by the elementary linear elastic approach.

3. Discussion of the J-integral approach

Path-independent integrals are used in physics to calculate the intensity of a singularity of a field quantity without knowing the shape of this field in the vicinity of the singularity. They are derived from conservation laws. For the singularity approach of structural materials, the J-integral (Rice integral) is applied as estimation or replacement of the energy release rate in the fictive non-linear elastic, region. According to the definition, is *J*, (near a crack singularity), the component along the crack-line of a vector integral, having a thinkable meaning of a rate of energy-release per unit crack-extension for not oblique and incipient self-similar growth of a crack in a (nonlinear) elastic material. Thus questionable for loading behavior of wood due to initial oblique crack extension and skipping across fibers. The path-independency of *J* can be established only, when the strain energy density of the material is a single valued function of strain. However, in a deformation theory of plasticity, (which does not apply for structural materials and viscous fluids), or in the fictive nonlinear elasticity theory for radial monotonic loading and no unloading, *J* still can be path-independent, but has not the meaning of energy-release rate. It is the total potential-energy difference between two identical and identically (monotonically) loaded cracked bodies which differ in crack lengths by a differential amount, (what represents a difference in absorbed, instead of released, energy). Further, in a flow theory of plasticity (as applies for wood and other structural materials as elastic-plastic materials), even under monotonic loading, no path-independence is possible and J tends to zero as the contour shrinks to the crack tip. The same applies for a growing crack in an elastic material. Under arbitrary load histories and at loading over the top of the lading curve, *J* is path-dependent, and even has not any physical meaning. The curved loading line and blunting of the top of the loading curve and formation of the fracture zone and the main amount of crack growth with crazing and small crack formation in, (and outside), the process zone, means unloading and non-proportional plastic deformation. The

by a contour integration obtained *J* integral, in a common elastic-plastic material, is path-dependent and tends to zero as the contour shrinks to the crack tip, thus does not exist. However it does exist in a rigid- perfect plastic material, called "far field *J*", and also exists (and is equal) as "deformation *J*" by assumed pure elastic energy, represented by the loading diagram of Fig. 3.22 of [8], although elastic energy is not involved in yield. Thus according to non-linear fracture mechanics, the same *J* -value is obtained in a rigid - plastic material and a fully elastic material, while it does not exists in a real elastic plastic material and not in an elastic material at crack propagation. (Thus not for linear elastic fracture mechanics). The analysis clearly is too empirical, based e.g. on the so called Ramberg-Osgood equation, which is a power law fitting curve of data which does not represent any theory or material property and may represent any equation. The power law is as old as the oldest research in the 19th century and it appears not possible to get rid of it. The *J* approach also is in conflict with molecular Deformation Kinetics (reaction rate kinetics) where the rate of change and differences in the rate of change are always determining for damage and other processes [2] and parameter estimation requires following complex loading-unloading histories.
The main error of non-linear fracture mechanics is the assumption of existence of critical energy release rates for each stress type, which act independently of each other, and thus violate compatibility conditions and violate the necessary mixed mode fracture criterion.

4. Exact solution of the "Boundary value problem" of fracture mechanics

4.1. Derivation of the so called "mixed I-II mode" fracture criterion

The analysis of the boundary value problem of fracture mechanics of isotropic material is e.g. discussed in ([5], § 8.9-10 and § 10.9). An extension for orthotropic materials, like wood and reinforced polymers, see § 5, is derived in [3]. Determining for a solution are the boundary conditions along the whole boundary of a crack in an infinite plate and at the far field boundary (at infinity). Then, the failure criterion depends on the actual ultimate uniaxial tensile stress at the crack boundary, which is the highest loaded material near or at the crack tip. The flat elliptic crack form can be seen as the accountable first expanded of any crack form. This form gives the highest stresses for any first expanded load, and thus delivers the highest, and thus the most probable, lower bound solution. The followed estimation of stresses around a flat elliptic hole, is based on the Airy stress function solution of [6]. This was a general accepted method in the past and recent past. See e.g. [7] for the failure criterion of concrete, covering the known data at that time. This exact analysis is now applied in rock

mechanics [5], and for wood (van der Put, iews.nl). There, the mathematical solution of the Airy stress function equation:

$$\nabla^2\left(\nabla^2 U\right)=0 \tag{4.1}$$

is given in terms of two analytic functions $\phi(z)$ and $\chi(z)$, (where $z=x+iy$), satisfying the

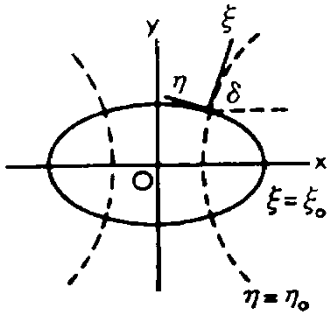

Figure 4.1. Elliptic hole and coordinates [3]

conditions at infinity and at the whole elliptic crack boundary surface, $\xi = \xi_o$, showing no discontinuity of displacements, thus being the solution. Thus:

$$U = R\left\{\bar{z}\phi(z)+\chi(z)\right\} = 0.5\left\{\bar{z}\phi(z)+z\overline{\phi}(z)+\chi(z)+\overline{\chi}(z)\right\} \tag{4.2}$$

The analytical functions (complex potentials) can be taken to be polynomials, or power series in 1/z, or Fourier series, all for suitable cases. It will be shown, see § 6.2, that all prescribed textbook equations: [8], [9], [10], [11] and [5] are based on the stress potential functions eq.(4.3) and eq.(4.4) of [6]. For the analysis of the elliptic crack, it is obvious to use elliptic coordinates, e.g. for giving stress boundary conditions along the whole crack boundary ξ_o and for the right crack tangent direction with the highest stress, for the exact solution.
For the elliptic hole $\xi = \xi_o$ with semi-axes: $a = c\cosh(\xi_o)$ and $b = c\sinh(\xi_o)$ in an infinite region loaded by an uniaxial stress p at infinity, inclined at β to the major axis Ox of the ellipse, (see Fig. 4.2, $a > b$), the functions $\phi(z)$ and $\chi'(z) = \psi(z)$ are, for an exact solution:

$$4\phi(z) = pce^{2\xi_0}\cos(2\beta)\cosh(\zeta)+pc\left(1-e^{2\xi_0+2i\beta}\right)\sinh(\zeta) \tag{4.3}$$

$$4\psi(z) = -pc[\cosh(2\xi_0)-\cos(2\beta)+e^{2\xi_0}\sinh\left(2\left(\zeta-\xi_0-i\beta\right)\right)]\cos ech(\zeta) \tag{4.4}$$

These equations (4.3) and (4.4) satisfy the required conditions at infinity and at the surface: $\xi = \xi_o$ of the elliptic hole. Using $dz / d\zeta = \omega'(\zeta) = c\sinh(\zeta)$, it follows that:

$$4\phi'(z) = 4\frac{d\phi}{d\zeta}\frac{d\zeta}{dz} = pe^{2\xi_0}\cos(2\beta)+p\left(1-e^{2\xi_0+2i\beta}\right)\coth(\zeta) \tag{4.5}$$

The tangential stress σ_t at the crack boundary $\xi = \xi_o$ is simply: $\sigma_t = \sigma_\eta$ because there: $\sigma_\xi = 0$, as boundary condition (Because the crack is empty there is no pressure and shear on the crack

boundary surface) and using eq.(4.5), and because:

$$\sigma_\xi + \sigma_\eta = 2\left[\phi'(z) + \bar{\phi}'(z)\right] = \sigma_t = 2\left[\phi'(\xi_0 + i\eta) + \phi'(\xi_0 - i\eta)\right] =$$

$$= pe^{2\xi_0}\cos(2\beta) + 0.5p\left(1 - e^{2\xi_0 + 2i\beta}\right)\coth(\xi_0 + i\eta) + 0.5p\left(1 - e^{2\xi_0 - 2i\beta}\right)\coth(\xi_0 - i\eta) =$$

$$= pe^{2\xi_0}\cos(2\beta) + p\left[\cosh(2\xi_0) - \cos(2\eta)\right]^{-1}\sinh(2\xi_0) +$$

$$- pe^{2\xi_0}\left[\cos(2\beta)\sinh(2\xi_0) + \sin(2\beta)\sin(2\eta)\right]\left[\cosh(2\xi_0) - \cos(2\eta)\right]^{-1} =$$

$$= p\frac{\sinh(2\xi_0) + \cos(2\beta) - \exp(2\xi_0)\cos(2(\beta - \eta))}{\cosh(2\xi_0) - \cos(2\eta)}\,, \tag{4.6}$$

eq.(4.6) follows and can be extended by combining two stresses at infinity: p_2 inclined at β to Ox and p_1 at $\pi/2 + \beta$, making any loading combination (σ_y τ_{xy}) possible, according to:

$\sigma_x = p_1\sin^2(\beta) + p_2\cos^2(\beta)$, $\sigma_y = p_1\cos^2(\beta) + p_2\sin^2(\beta)$, $\tau_{xy} = -0.5(p_1 - p_2)\sin(2\beta)$ giving:

$$\sigma_t = \frac{2\sigma_y\sinh(2\xi_0) + 2\tau_{xy}[(1 + \sinh(2\xi_0))\cot(2\beta) - \exp(2\xi_0)\cos(2(\beta - \eta))\cos ec(2\beta)]}{\cosh(2\xi_0) - \cos(2\eta)} \tag{4.7}$$

For a flat crack, thus for small ξ_0 and η (near the crack tip) this is:

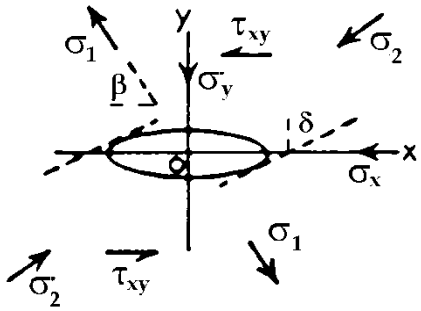

Figure 4.2. - Stresses in the notch plane Ox, [3].

$$\sigma_t = \frac{2\left(\xi_0\sigma_y - \eta\tau_{xy}\right)}{\xi_0^2 + \eta^2} \tag{4.8}$$

The maximal tangential stress follows from $d\sigma_t/d\eta = 0$. Thus:

$$\tau_{xy}\left(\xi_0^2 - \eta^2\right) + 2\xi_0\sigma_y\eta = 0 \quad \rightarrow \quad \eta = \xi_0\left[\sigma_y \pm \sqrt{\left(\sigma_y^2 + \tau_{xy}^2\right)}\right]/\tau_{xy}\,. \tag{4.9}$$

Substitutions in eq.(4.8) gives:

$$\xi_0\sigma_t = \sigma_y \pm \sqrt{\left(\sigma_y^2 + \tau_{xy}^2\right)} \tag{4.10}$$

This equation can be written:

$$\left(\xi_0\sigma_t - \sigma_y\right)^2 = \left(\pm\sqrt{\left(\sigma_y^2 + \tau_{xy}^2\right)}\right)^2 = \sigma_y^2 + \tau_{xy}^2\,, \quad \rightarrow$$

$$\frac{\tau_{xy}^2}{(\xi_0\sigma_t)^2}+\frac{\sigma_y}{\xi_0\sigma_t/2}=1 \qquad (4.11)$$

Transformation from elliptic to confocal polar coordinates, by eq.(6.5) below, gives:

$$\xi_0=\sqrt{2r_0/c}\cdot\cos(\delta)\approx\sqrt{2r_0/c} \qquad (4.12)$$

and substitution in eq.(4.11) gives, for variable c, with constant $\sigma_t\,(r_o)^{1/2}$:

$$\frac{\sigma_y\sqrt{\pi c}}{\sigma_t\sqrt{\pi r_0/2}}+\frac{\left(\tau_{xy}\sqrt{\pi c}\right)^2}{\left(\sigma_t\sqrt{2\pi r_0}\right)^2}=\frac{K_I}{K_{Ic}}+\frac{K_{II}^2}{(K_{IIc})^2}=1 \qquad (4.13)$$

what is the mixed I-II mode fracture criterion, while eq.(4.11), with constant $\xi_o\cdot\sigma_t$ thus with a structural constant initial focal distance $2c$ of clear wood, which for initial sharp flat cracks is about equal to the crack length $2a$, gives and explains, the uniaxial, ultimate strength criterion for clear wood. Because the high value of σ_t and small value of the crack tip distance r_o, are not determined by eq.(4.13), only the product $\sigma_t\,(r_o)^{1/2}$, is obtained. The distance r_o from the focus of the elliptical crack to the adjacent critical crack tip boundary where crack extension proceeds, is small for flat cracks (when $a >> b$). Thus the high cohesion strength σ_t is reached, what is possible because of the indefinitely high strength of the 3-dimensional hydrostatic stress state at the crack tip. (see paragraph 4.2)

Besides the crack length, the crack width, is determined by the focus distances. The mode I crack tip opening displacement (CTOD) δ_o, for plane strain, is according to textbooks:

$\delta_o = 2(K_I)^2/(\pi\sigma_y E)$.

This can be written: $\delta_o = 2(K_I)^2/\pi\sigma_y E = 2(\sigma_y)^2(\pi r_o/2)/\pi\sigma_y E = r_o\,\sigma_y/E = r_o\,\varepsilon_y$.

Thus the CTOD at first yield δ_o is proportional to r_o and thus is very small for flat cracks.

According to eq.(4.12) is $\xi_o = \sqrt{(2r_o/c)} \approx \sqrt{(2r_o/a)}$ and is, as ellipse, also equal to: $\xi_o = b/a$.

Thus is: $r_o = b^2/2a$. The radius ρ of the elliptic curvature of the crack tip at x = a is: $\rho = b^2/a$.

Thus is: $\rho = 2\,r_o$, and $2r_o$ in eq.(4.13) can be replaced by ρ, giving the influence of the sharpness of the crack tip. Because of this is mentioned in literature that even a small crack with a sub-micron tip radius can amplify stresses several hundred times causing structural failure under relatively low average stress (despite the high hydrostatic strength).

According to eq.(4.11) is the highest stress for mode I failure at the crack tip:

$\sigma_y = \sigma_t\cdot\xi_o/2 = \sigma_t\cdot\sqrt{(r_o/2c)} = \sigma_t\cdot\sqrt{(\rho/4a)}$,

what is identical to the result of the oldest derivation by Inglis in 1913, (also applied by Griffith to evaluate his strain energy), because, according to Inglis, is for mode I failure:

$\sigma_t = \sigma_y(1+2\sqrt{(a/\rho)}) \approx 2\,\sigma_y\sqrt{(a/\rho)}$ for flat cracks. Thus, reversed: $\sigma_y \approx \sigma_1\sqrt{(\rho/4a)}$ the same as

the exact result eq.(4.11). The derivation of Inglis for mode I failure is now extended for mixed mode failure by eq.(4.13), which is equal to the empirical Wu-equation. Wu noticed a crack jumping over fibers, what is identical to fracture propagation at an alternate changing, but small, value of (+ and -) δ, which thus is neglected as best value (Thus $\cos(\delta) \approx 1$). As shown later, fracture always ends at δ close to zero by failure of the developed remaining hydrostatic bonds in the end state. For clear wood and short rectangular notches however oblique crack extension is possible as is measured and what is discussed in [3].
Eq.(4.13), as exact equation, also follows from the critical distortional energy principle [3], thus also applies for initial flow before building up a hydrostatic stress field.
Notice that no critical energy criterium is possible or required to obtain $K_I, K_{II}, K_{Ic}, K_{IIc}$.

4.2. Derivation of the hydrostatic stress state for fracture

Eq.(4.13) shows that fracture mechanics with constant stress intensity:

$$K_{Ic} = \sigma_y \sqrt{\pi c_c} = \sigma_t \sqrt{\pi r_0 / 2} \tag{4.14}$$

applies when r_o and σ_t are constant. Thus σ_t represents the cohesion strength at the crack tip craze and $2r_o$ is the invariant radius of the constant dimensions of the, "fracture process zone" called craze, at the crack tip. This zone clearly represents a kind of crazing with, as such, an invariant size, (which is regarded to be related to a material inhomogenities structure). The, at the upper crack tip, also occurring hydrostatic tension as shown by eq.(6.18), for pure mode I tensile loading perpendicular to the crack direction, gives:

$$\sigma_r = \sigma_\theta = p\sqrt{c / 2r} \qquad (\tau_{xy} = 0) \tag{4.15}$$

This is equal to the third stress σ_z of triaxiality, due to confined contraction, with $\nu = 0.5$ for no volume change as lower bound solution. Thus:

$$\sigma_z = \nu\sigma_r + \nu\sigma_\vartheta = \sigma_r = \sigma_\theta \tag{4.16}$$

This probably shows the start of extension of the process zone independent of the final fracture according to eq.(4.14). This means, that, by early yield, the local hydrostatical stresses may, as such, be undetermined high, (when $r \rightarrow 0$), without failure in the isotropic wood matrix (lignin with branched hemicellulose). Eq.(4.15) gives the exact property of the hydrostatic ultimate stress to be proportional to $(r_o)^{-1/2}$ at yield. Thus:

$$\sigma_t = K_c / \sqrt{2\pi r_0} \tag{4.17}$$

where K_c = constant; $r_o << c$, according to eq.(4.12) because $\xi_o << 1$ for flat cracks. It is thus not true, although stated in textbooks, that:

$$K_I \neq \lim_{r\to 0,\theta=0}(\sigma_2 \cdot \sqrt{2\pi r}) \tag{4.18}$$

because $\{\sigma_2 \cdot \sqrt{(2\pi r)}\}$ is independent of *r*. Thus this limit does not exist. It is the hydrostatic stress which explains why the stress may become high when *r* is small. This is determined by the amount of stress spreading by the stress spreading law. See Appendix of [12] for the derivation. Finally not eq.(4.15) but eq.(4.14) determines total failure and the failure criterion. Early failure, by hydrostatic eq.(4.15), should be visible by an almost pure collinear crack extension.

Based on the potentials eq.(4.3) and eq.(4.4) all stresses everywhere in the field around the crack can be calculated. See Fig. 6.2 for the result. And also the stress transformations are known. Because:

$$\sigma_\xi + \sigma_\eta = \sigma_x + \sigma_y = 2\left[\phi'(z) + \bar{\phi}'(z)\right] \tag{4.19}$$

$$\sigma_\eta - \sigma_\xi + 2i\tau_{\xi\eta} = (\sigma_y - \sigma_x + 2i\tau_{xy})e^{2i\delta} = 2[\bar{z}\phi''(z) + \psi'(z)][\omega'(\zeta)/\bar{\omega}'(\zeta)] \tag{4.20}$$

τ_{xy} is known from the imaginary part of eq.(4.20) and $\sigma_y - \sigma_x$ from the real part.

Thus with eq.(4.19), all stresses are known in Cartesian coordinates. The same is possible for transformation to polar coordinates.

For pure shear loading along the crack, the exact equations, in elliptical coordinates, also show the presence of hydrostatic stress at the top of the crack tip as is shown by the following derivation. By loading in pure shear, thus by loading by two principal stresses at infinity of *p* at $\beta = \pi/4$ and - *p* at $\beta = 3\pi/4$, the stresses are:

$$\sigma_\xi = p\left(\cosh(2\xi) - 1\right)\left(\alpha - \alpha^2\right)\sin(2\eta) \tag{4.21}$$

$$\sigma_\eta = p\left[\alpha^2\left(\cosh(2\xi) - 1\right) - \alpha\left(\cosh(2\xi) + 1\right)\right]\sin(2\eta) \tag{4.22}$$

$$\tau_{\xi\eta} = p\left[\alpha\cos(2\eta) - \alpha^2\left(1 - \cos(2\eta)\right)\right]\sinh(2\xi) \tag{4.23}$$

where $\alpha = 1/[\cosh(2\xi) - \cos(2\eta)]$. This delivers a hydrostatic stress state when: $\sigma_\xi = \sigma_\eta$, are equal principal stresses, and when, necessarily, also: $\tau_{\xi\eta} = 0$. For: $\sigma_\xi = \sigma_\eta$ is:

$$\left(\alpha - \alpha^2\right)\cosh(2\xi) - \alpha + \alpha^2 = -\left(\alpha - \alpha^2\right)\cosh(2\xi) - \alpha^2 - \alpha \quad \rightarrow \cosh(2\xi) = \frac{\alpha}{\alpha - 1} \tag{4.24}$$

and for $\tau_{\xi\eta} = 0$ is:

$$\alpha\cos(2\eta) - \alpha^2 + \alpha^2\cos(2\eta) = 0 \quad \rightarrow \cos(2\eta) = \frac{\alpha}{\alpha + 1} \tag{4.25}$$

Substitution of eq.(4.24) and (4.25) into the stress equations (4.21) and (4.22), gives:

$$\sigma_\xi = \sigma_\eta = -p\alpha \sin(2\eta) = -p\alpha \frac{\sqrt{1+2\alpha}}{1+\alpha} \approx -p\sqrt{2\alpha} = -p\sqrt{\frac{c}{2r}} \tag{4.26}$$

because $\alpha = (c/4r) >> 1$, where c is half the crack length. The third principal stress is:

$$\sigma_z = \upsilon\sigma_\xi + \upsilon\sigma_\eta = 0.5(\sigma_\xi + \sigma_\eta) = \sigma_\xi = \sigma_\eta \tag{4.27}$$

The exact equations (4.19 to 4.21) in elliptical coordinates, thus show, that also at pure shear loading along the crack length, a hydrostatic ultimate stress occurs at the crack tip. In the limit at the same place and magnitude as for pure mode I loading. This therefore also applies for any load combination. According to the critical distortional energy principle this may provide an indefinitely high strength to cover the high singularity stress. (For dominating tensional loading the sign of p, and thus of α, has to be reversed in this analysis). According to eq.(6.7) is: $\alpha = c/4r$ in polar coordinates. The, in elliptical coordinates derived, hydrostatic stress for pure shear loading, is not found when the same derivation is done after transformation to confocal polar coordinates of the exact elliptic coordinate equations. The reason is that this transformation is not right and only applies for small values of the variables thus $\theta \approx 0$, thus only for mode I failure. Thus the Textbook equation for pure shear loading is not right. This is discussed in § 6.1. As well the original derivation in [5], as the Textbook modification in [8], don't account for the kink $\delta = \theta/2$ in Fig. 6.1 and thus their equations only can apply for $\theta = \delta = 0$. Thus only for mode I failure. The in elliptical coordinates derived, hydrostatic stress for pure tensional loading perpendicular to the crack (see eq.(8.219 to (8.221) of Jaeger et all) for $\beta = \pi/2$, and small values of ξ and η, thus close to crack tip, shows indeed: $\sigma_\xi \approx \sigma_\eta$ and $\tau_{\xi\eta} \approx 0$ of the hydrostatic stress state, confirming the small variable derivation of § 6.1 for tension perpendicular to the crack direction. The order of the stresses σ_ξ and σ_η is: $p\cdot(2\xi)/(\xi^2 + \eta^2)$, thus one order higher than the order of p, showing the peak stresses of fig. 6.2. Besides hydrostatic stress at the crack tip craze, also slip- line analysis between and around rows of small cracks, show that also by apparent shear flow, hydrostatic normal stress increase occurs due to the stress spreading effect. For local compressional loading, the strong increase of strength, due to confined dilation and necessary hydrostatical stress state, is generally known. See [12], for the exact derivation by the "slip- or shear- line" theory. For compatible displacements, shear lines are straight, or curved according to the logarithmic spiral. The strength calculation method, based on this spiral stress spreading, was already in the Dutch building code. The orthotropic extension of the critical distortional energy principle, as basis for orthotropic hydrostatic stress calculation, is

given in [3] Ap. B. High hydrostatic *tension* also is measured, in materials. Measured is e.g. 60 atmospheres for tension of water in a glass tube. Crazing, by hydrostatic tension in the process zone, is known to be typical for amorphous material, thus applies for the isotropic wood matrix. The derivation shows that this is a general property of fracture.

5. Empirical verification of the mixed I-II mode fracture criterion of wood

For isotropic material eq.(4.13) predicts that $K_{IIc} = 2\,K_{Ic}$. This is e.g. verified for Balsa wood, which is elastic orthotropic, but is extremely light, thus has a very low density of reinforcement, and thus, the isotropic matrix is determining for the strength showing the isotropic strength behavior by $K_{IIc} = 2\,K_{Ic}$ as verified by the data of Wu on Balsa (by $K_{IIc} \approx 140$ psi.in$^{0.5}$ and $K_{Ic} \approx 60$ psi.in$^{0.5}$; (where $K_{IIc} \geq 2\,K_{Ic}$ by some hardening in the mode II test, and $K_{Ic} \leq K_{IIc}/2$ by early instability of the tension test).

The Wu- equation is generally applicable, also when σ_y is a compression stress, as verified by the measurements. When the compression is high enough to close small notches ($\sigma_{y,cl} \approx 2G_{xy}\xi_o$), τ_{xy} has to be replaced by the effective shear stress:

$$\tau^*_{xy} = \tau_{xy} + \mu\left(\sigma_y - \sigma_{y,cl}\right),$$

where μ is the friction coefficient, giving:

$$1 = \frac{\sigma_{y,cl}}{\xi_0\sigma_t/2} + \frac{\left(\tau^*_{xy}\right)^2}{\xi_0^2\sigma_t^2}, \qquad (5.1)$$

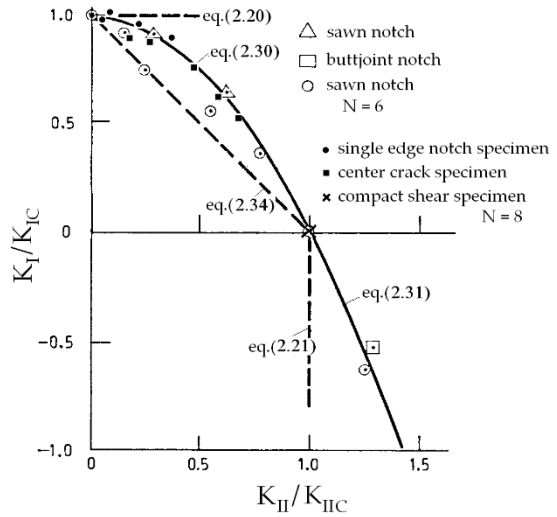

Figure 5.1. Equation numbers are of the first edition of [3]

eq.(2.31) = (5.1); eq.(2.30) = (4.13)

what is fully able to explain fracture by compression perpendicular to the notch plane.
The stress strain relations for orthotropic stresses in denser wood, can be given by:

$$\varepsilon_x = c_{11}\sigma_x + c_{12}\sigma_y ; \quad \varepsilon_y = c_{12}\sigma_x + c_{22}\sigma_y ; \quad \gamma_{xy} = c_{66}\tau_{xy} . \tag{5.2}$$

Substitutions of eq.(5.2):

$$\varepsilon_x = c_{11}\frac{\partial^2 U}{\partial y^2} + c_{12}\frac{\partial^2 U}{\partial x^2} , \text{ …….etc.}$$

in the compatibility condition:

$$\frac{\partial^2 \varepsilon_x}{\partial y^2} + \frac{\partial^2 \varepsilon_y}{\partial x^2} = \frac{\partial^2 \gamma_{xy}}{\partial x \partial y} , \tag{5.3}$$

gives:

$$c_{22}\frac{\partial^4 U}{\partial x^4} + \left(c_{66} + 2c_{12}\right)\frac{\partial^4 U}{\partial x^2 \partial y^2} + c_{11}\frac{\partial^4 U}{\partial y^4} = 0 \tag{5.4}$$

Wood acts as a reinforced material and can be treated to contain e.g. a shear-reinforcement and an additional tensile reinforcement in the main direction. The reinforcement in y-direction with the same amount in x-direction is accounted to the isotropic matrix.
Then, for equilibrium of the matrix stresses (expressed in the total stresses) applies:

$$\frac{\sigma_x}{n_1} = \frac{\partial^2 U}{\partial y^2} ; \quad \sigma_y = \frac{\partial^2 U}{\partial x^2} ; \quad \frac{\tau_{xy}}{n_6} = -\frac{\partial^2 U}{\partial x \partial y} , \tag{5.5}$$

Inserted in the compatibility equation, eq.(5.3), this should give the isotropic Airy tress function. But the same compatibility should apply for matrix and reinforcement. Thus inserting the total stresses in eq.(5.3) should give a proportional result, given by eq.(5.6):

$$c_{22}\frac{\partial^4 U}{\partial x^4} + \left(n_6 c_{66} + (1+n_1)c_{12}\right)\frac{\partial^4 U}{\partial x^2 \partial y^2} + n_1 c_{11}\frac{\partial^4 U}{\partial y^4} = 0 \tag{5.6}$$

For the isotropic matrix thus is:

$$n_1 c_{11} / c_{22} = 1 ; \quad (n_6 c_{66} + \left(1+n_1\right)c_{12}) / c_{22} = 2 ,$$

giving:

$$\frac{\partial^4 U}{\partial x^4} + 2\frac{\partial^4 U}{\partial x^2 \partial y^2} + \frac{\partial^4 U}{\partial y^4} = \nabla^2(\nabla^2 U) = 0 \qquad \rightarrow \tag{5.6}$$

$$n_1 = \frac{c_{22}}{c_{11}} = \frac{E_x}{E_y} ; \qquad n_6 = \left(2 - \frac{c_{12}}{c_{22}} - \frac{c_{12}}{c_{11}}\right)\cdot\frac{c_{22}}{c_{66}} = \left(2 + \nu_{21} + \nu_{12}\right)\cdot\frac{G_{xy}}{E_y} \tag{5.7}$$

This orthotropic-isotropic transformation of the Airy stress function in the elastic state of the reinforcement and the calculation method based on the stresses of the matrix makes it

possible to use the isotropic solutions of *U* to find the matrix stresses (which should not surmount the matrix strength). In this way eq.(4.13) becomes in total orthotropic stresses:

$$1 = \frac{\sigma_y}{\xi_0 \sigma_t / 2} + \frac{\tau_{iso}^2}{\xi_0^2 \sigma_t^2} = \frac{\sigma_y}{\xi_0 \sigma_t / 2} + \frac{\tau_{ort}^2}{\xi_0^2 \sigma_t^2 n_6^2} = \frac{K_I}{K_{Ic}} + \frac{(K_{II})^2}{(K_{IIc})^2} \tag{5.8}$$

and it follows that:

$$\frac{K_{IIc}}{K_{Ic}} = \frac{\xi_0 \sigma_t n_6}{\xi_0 \sigma_t / 2} = 2n_6 \tag{5.9}$$

$$2n_6 = 2\left(2 + \nu_{21} + \nu_{12}\right) \cdot G_{xy} / E_y = \tag{5.10}$$

= 2(2 + 0.57)/0.67 = 7.7 for Spruce and: 2(2 + 0.48)/0.64 = 7.7 for Douglas Fir in TL-direction, according to data of [11]. This is, in this chosen example, independent of the densities of respectively 0.37 and 0.50 at a moisture content of 12 %. Thus, for $K_{Ic} \approx$ 265 kN/m$^{1.5}$, is K_{IIc} = 7.7x265 = 2041 kN/m$^{1.5}$ in TL-direction. In RL-direction this factor is 3.3 to 4.4. Thus, when K_{IIc} is the same as in the TL-direction, the strength in RL-direction is predicted to be a factor 1.7 to 2.3 higher, with respect to the TL-direction. This however applies at high crack velocities ("elastic" failure) and is also dependent on the site of the notch. At common loading rates a factor lower than 410/260 = 1.6 is measured and at still lower cracking speeds, this strength factor is expected to be about 1 when fracture is in the "isotropic" middle lamella. It then thus is independent of the TL and RL-direction according to the local stiffness and rigidity values. To know the mean influence, it is necessary to analyze fracture strength data dependent on the density and the elastic constants of n_6. From the rate dependency of the strength follows an influence of viscous and viscoelastic processes. This has to be analyzed by Deformation Kinetics theory, see [2].

Table 1. - Lack of fit values for supposed failure criteria [13]

Failure criterion	*p*-value
$K_I / K_{Ic} = 1$	0.0001
$K_I / K_{Ic} + K_{II} / K_{IIc} = 1$	0.0001
$K_I / K_{Ic} + (K_{II} / K_{IIc})^2 = 1$	0.5629
$(K_I / K_{Ic})^2 + K_{II} / K_{IIc} = 1$	0.0784
$(K_I / K_{Ic})^2 + (K_{II} / K_{IIc})^2 = 1$	0.0001

Empirical verification of the above derived theory equation, eq.(5.8), which is a Coulomb equation, often called Wu-equation for wood, is not only obtained by Wu, [14], but also by tests of Mall et al [13] done at the TL-system on eastern red spruce at normal climate conditions using different kinds of test specimens. The usual finite element simulations provided the geometric correction factors, and the stress intensity factors. The lack of fit test was performed on these data, at the for wood usual variability, assuming the five different, often suggested empirical failure equations of Table 1. The statistical lack of fit values in the table show, that only the Wu-failure criterion, the third equation of Table 1, cannot be rejected due to lack of fit. This does not apply for the precise empirical fits by the other equations and that is the reason why this lack of fit test never is performed by empirics. The Wu-equation is shown to fit also clear wood and timber strength data in [1], [15] and [3], as to be expected from theory.

6. Comparison of the exact solution with the applied textbook equations.

6.1. Transformation to confocal coordinates of the elliptic equations

The general accepted textbook analysis method (see Appendix of [8]) is based on crack tip singularity equations, very close to the crack tip singularity, and not on the boundary value approach along the whole crack length of § 4. These singularity equations, given in [5] – §8.10, are also based on the Airy stress function solution of Stevenson [6], but simplified to only apply at very small, lower order distances r to the crack tip. It will be shown, in the following, that also only lower order values of θ apply. However, due to the applied modification of (Appendix 2 of Anderson [8]) they are wrongly also applied for higher order distances and any rotation. To diminish the distortion of the equations at higher values of θ, all textbooks wrongly removed the kink between radius r and the normal in Fig. 6.1, taking the lower $\delta = \theta$, and the upper $\delta = 0$. Further, the textbook expressions, also wrongly, are split into two independent loading cases. One for normal stress loading perpendicular to the crack direction alone, and the other for shear stress loading along the crack direction alone. Although these solutions exclude each other and cannot apply at the same time, they are put together as one solution, as if they are coherent loading components. This assumption clearly is based on an old believe in the existence of independent separate failure modes. The general mixed mode solution of this boundary value problem shows however that this incompatible solution can not be right. The modes act, alone, as special loading cases of the general mixed

mode failure case. The right singularity equations of [5] – §8.10, will be discussed and extended in the following. The stresses outside the crack boundary also follow from the solution of the Airy stress function of § 4.2.

For a point near the elliptic crack tip: $\xi = \xi_o$, with coordinates:

$$x = c\cosh(\xi)\cos(\eta), \quad y = c\sinh(\xi)\sin(\eta), \tag{6.1}$$

with the focus $x = c$ of the flat ellipse as new origin for Cartesian coordinates X, Y, (see Fig. 6.1) which are for small values of ξ and η:

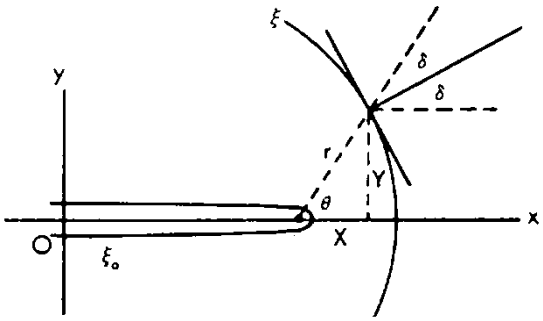

Figure 6.1.- Confocal polar coordinates for transformation of the elliptical crack coordinates to polar crack tip coordinates.

$$X = x - c = c\left(\xi^2 - \eta^2\right)/2, \quad Y = y = c\xi\eta \tag{6.2}$$

what is, in polar coordinates:

$$r = \sqrt{X^2 + Y^2}, \quad X = r\cos(\theta), \quad Y = r\sin(\theta), \tag{6.3}$$

From (6.2) follows:

$$\xi^2 + \eta^2 = 2\left(X^2 + Y^2\right)^{1/2}/c = 2r/c \tag{6.4}$$

And from (6.2) and (6.4) follows for the elliptic coordinates:

$$\xi = (r/c)^{1/2}\left(1 + \cos(\theta)\right)^{1/2} = (r/c)^{1/2}\cos(\theta/2) \tag{6.5}$$

$$\eta = (r/c)^{1/2}\left(1 - \cos(\theta)\right)^{1/2} = (r/c)^{1/2}\sin(\theta/2) \tag{6.6}$$

The quantity α of eq.(4.6) and (4.7) becomes:

$$\alpha = \left(\cosh(2\xi) - \cos(2\eta)\right)^{-1} = 0.5\left(\xi^2 + \eta^2\right)^{-1} = c/4r \tag{6.7}$$

The angle δ follows by:

$$e^{2i\delta} = \omega'(\zeta)/\bar{\omega}'(\zeta) = \left(\sinh(\xi + i\eta)\right)/\left(\sinh(\xi - i\eta)\right) = (\xi + i\eta)/(\xi - i\eta) = e^{i\theta} \tag{6.8}$$

or: $\delta = \theta/2$ (6.9)

Using this, but ignoring eq.(6.9), is:

$$\sigma_x + \sigma_y = \frac{\partial^2 U}{\partial x^2} + \frac{\partial^2 U}{\partial y^2} = 2\left[\phi'(z) + \bar{\phi}'(z)\right] = 4R\left[\phi'(z)\right], \tag{6.10}$$

what is, for the flat crack $\xi_0 = 0$, for loading by stress p at infinity at an angle β to the crack, using the small values properties:

$$\sigma_r + \sigma_\theta = \sigma_\xi + \sigma_\eta = p\cos(2\beta) + \alpha p\left[\left(1-\cos(2\beta)\right)\sinh(2\xi) - \sin(2\beta)\sin(2\eta)\right] =$$

$$= p\cos(2\beta) + \alpha p\left[\left(1-\cos(2\beta)\right)(2\xi) - (2\eta)\sin(2\beta)\right] =$$

$$= p\cos(2\beta) + p(c/2r)^{1/2}\left[\left(1-\cos(2\beta)\right)\cos(\theta/2) - \sin(2\beta)\sin(\theta/2)\right] \tag{6.11}$$

The first term is constant and regarded to be negligible with respect to the term in $(r)^{-1/2}$. This means that $\sqrt{(c/r)}$ is of a higher order and thus r is two orders smaller than half the crack length c. It is important to notice the small allowable value of r, which is (r < 2c/100), thus 1/100 times the crack length 2c. This is not noticed and not applied in practice and stresses are regarded to be of the same order of p.

Stresses are known from equivalent derivatives of the whole crack boundary problem solution, discussed at § 4. It applies that:

$$\tau_{xy} = -\frac{\partial^2 U}{\partial x \partial y} = -0.5\left\{i\bar{z}\phi''(z) - iz\bar{\phi}'' + i\chi''(z) - i\bar{\chi}''(z)\right\} \tag{6.12}$$

$$\sigma_y - \sigma_x + 2i\tau_{xy} = \frac{\partial^2 U}{\partial x^2} - \frac{\partial^2 U}{\partial y^2} - 2i\frac{\partial^2 U}{\partial x \partial y} = 2\left\{\bar{z}\phi''(z) + \chi''(z)\right\} \tag{6.13}$$

$$\sigma_x + \sigma_y = \frac{\partial^2 U}{\partial x^2} + \frac{\partial^2 U}{\partial y^2} = 2\left[\phi'(z) + \bar{\phi}'(z)\right] = 4R\left[\phi'(z)\right], \tag{6.14}$$

what leads, similar to eq.(6.11), after transformation to confocal polar coordinates, to:

$$\left(8r/(cp^2)\right)^{1/2}\sigma_r = \sin(\theta/2)\cdot\left(1-3\sin^2(\theta/2)\right)\sin(2\beta) + 2\cos(\theta/2)\cdot\left(1+\sin^2(\theta/2)\right)\sin^2(\beta) \tag{6.15}$$

$$\left(8r/(cp^2)\right)^{1/2}\sigma_\theta = -3\sin(\theta/2)\cdot\cos^2(\theta/2)\cdot\sin(2\beta) + 2\cos^2(\theta/2)\cdot\sin^2(\beta) \tag{6.16}$$

$$\left(8r/(cp^2)\right)^{1/2}\tau_{r\theta} = \cos(\theta/2)\cdot\left(3\cos^2(\theta/2)-2\right)\cdot\sin(2\beta) + 2\cos^2(\theta/2)\cdot\sin(\theta/2)\cdot\sin^2(\beta) \tag{6.17}$$

For the common mode I test with collinear crack propagation is: $\beta = \pi/2$ and $\theta = 0$.

Then is: $(8r/(cp^2))^{1/2}\sigma_r = 2$ and $(8r/(cp^2))^{1/2}\sigma_\theta = 2$, and $\tau_{r\theta} = 0$. Thus is:

$$\sigma_r = \sigma_\theta = p\sqrt{c/2r}\,. \tag{6.18}$$

showing, by the equal principal stresses and zero shear stress, the local hydrostatic tension.

Thus an undetermined high stress is possible. This is discussed at eq.(4.15).

In general, for pure mode I, thus $\beta = \pi/2$, follows:

$$(2r/c)^{1/2}\,\sigma_r = p\cos(\theta/2)\cdot\left(1+\sin^2(\theta/2)\right) \tag{6.19}$$

$$(2r/c)^{1/2}\,\sigma_\theta = p\cos^3(\theta/2)\cdot \tag{6.20}$$

$$(2r/c)^{1/2}\,\tau_{r\theta} = p\cos^2(\theta/2)\sin(\theta/2) \tag{6.21}$$

There is an extreme $\partial\sigma_\theta/\partial\theta = 0$, giving:

$$(2r/c)^{1/2}\,\partial\sigma_\theta/\partial\theta = -(3/2)p\cos^2(\theta/2)\cdot\sin(\theta/2) = 0\,,\ \rightarrow\ \theta = 0 \tag{6.22}$$

Thus the extreme stress is the hydrostatic stress at $r = r_o$:

$$p\sqrt{\pi c} = \sigma_t\sqrt{2\pi r_0} \tag{6.23}$$

Thus, as confirmed in the following derivation, also θ is a lower order small variable, close to zero, just like r, where r_o the minimum value of r, is the distance from the focus to the crack boundary where fracture proceeds. The transformation gives the transformation to r and θ of polar coordinates of the elliptical crack boundary, but for the increasing rotation with $\delta = \theta/2$ (according to eq.(6.5)), it follows from Fig.6.1 that:

$$\frac{r\,d\theta}{dr} = tg(\delta) = tg(\theta/2) \rightarrow \frac{d(\theta/2)}{tg(\theta/2)} = \frac{dr}{2r} = \frac{d\left(r/r_{\theta=0}\right)}{2\left(r/r_{\theta=0}\right)} = \frac{d\sin(\theta/2}{\sin(\theta/2)} = d\ln\sin(\theta/2) =$$

$$= (1/2)\cdot d\ln(r/r_{\theta=0}) = d\ln(r/r_{\theta=0})^{1/2} \quad \rightarrow \ln\left(\sin\left(\theta/2\right)\right) = \ln\sqrt{r/r_{\theta=0}} + C_1 \rightarrow$$

$$\rightarrow \sin\left(\theta/2\right) = \sqrt{r/r_{\theta=0}}\cdot e^{C_1} \quad \rightarrow\ \sin(\pi/2) = 1 = \sqrt{2c/r_{\theta=0}}\cdot e^{C_1} \rightarrow e^{C_1} = \sqrt{r_{\theta=0}/2c} \rightarrow \tag{6.24}$$

because for $\theta = \pi$, is $r = 2c$, the total crack length. It thus follows that then:

$$\sin\left(\theta/2\right) = \sqrt{r/2c} \tag{6.25}$$

But, because $r << 2c$, also θ has to be very small, close to $\theta = 0$, for a right applicable value. This is satisfied for mode I, thus for pure tension perpendicular to the crack, but not for pure shear along the crack.

The loading case, for pure shear S, follows from eq.(6.15 to 6.17) by the combination of two stresses of $p = S$ at $\beta = \pi/4$ with $p = -S$ at $\beta = 3\pi/4$ giving:

$$(2r/c)^{1/2}\,\sigma_r = S\sin(\theta/2)\cdot\left(1-3\sin^2(\theta/2)\right) \tag{6.26}$$

$$(2r/c)^{1/2}\,\sigma_\theta = -3S\sin(\theta/2)\cos^2(\theta/2) \tag{6.27}$$

$$(2r/c)^{1/2}\,\tau_{r\theta} = S\cos(\theta/2)\cdot\left(3\cos^2(\theta/2)-2\right) \tag{6.28}$$

As small variables solution, thus at $\theta = 0$, is:

$$\tau_{r\theta}\sqrt{2\pi r} = S\sqrt{\pi c} = \sigma_t\sqrt{2\pi r}$$

This satisfies the failure criterion eq.(4.13) for pure shear failure. However it is a trivial solution because the other 2 stresses are zero. And for $\theta = \pi$, no anti-symmetric solution is satisfied because then: $\sigma_r = -2S\sqrt{(c/2r)}$, $\sigma_\theta = 0$, and $\tau_{r\theta} = 0$. But, at the crack-boundary, σ_θ is never zero and σ_r is mostly zero or equal to σ_θ at the crack tip.

According to the exact approach of § 4, applies for initial failure by the ultimate tensile stress at the crack boundary: $\sigma_r = \tau_{r\theta} = 0$ and $\sigma_\theta = \sigma_t$. This is the case for eq.(6.26) to eq.(6.28) at $\theta = 35^0$, what is not a small value of θ close to zero. Thus the small variable solution, by this crack tip strength model, is not able to give the extreme values and is not able to satisfy eq.(6.9) for $\theta \neq 0$. All results further apply only for infinite long cracks because $r << c$. The equations are nevertheless applied by Textbooks for much higher values of even: $r >> 2c$, going to infinity. Clearly the small variables crack tip singularity approach is not a general approach and should not be used anymore and be removed from Textbooks. Only the Stevenson, crack boundary value solution, along the whole crack length, remains as only right solution, covering also the whole field around the crack. See Fig. 6.2 for the right stresses and [5] for the most extended description.

6.2. Proof of the identity of the textbook- and transformed exact equations

An extended proof is given because, for a scientific proof, all steps of a derivation have to be directly understandable for the reader, or else, reference to such a derivation has to be given. In textbooks, only stresses near the crack-tip, as singularity, are regarded. The solution of the so simplified boundary value problem is further based on the arbitrary believe (Irwin) that the sum of 3 separate, independently acting, fracture modes are determining for strength behavior. This is e.g. given in [10] and [8] - Appendix 2, whereto most textbooks refer, as e.g. [9] and RILEM state of the art report [11].

The exact boundary value solution, based on complex potentials of Stevenson [6], which as elliptic type differential equation, applies for equilibrium problems, is given in elliptic coordinates, making it easy to give the necessary stress boundary condition along the whole flat elliptic crack boundary. The solution gives the mixed I-II mode fracture criterion (e.g. for wood) which, when given in polar or Cartesian coordinates, is a simple expression, eq.(4.13), for the determining two dimensional problem of a flat crack. It is shown, by the derivation below, that the generalized transformation, from elliptical, to confocal polar coordinates, for pure mode I loading, eq.(6.19) to eq.(6.21) and for pure mode II loading, eq.(6.26) to

eq.(6.28), are taken together, in one equation, as if interaction is possible of these two, each excluding, pure mode solutions. Thus the exact solution for mode I loading alone, when the shear loading is zero, is combined with the exact solution for shear loading alone, when the tensile loading is zero, what means that a not compatible equilibrium system is regarded for low enough stresses near the crack tip singularity. This solution, satisfying no crack boundary and failure conditions can not be regarded as a lower bound solution of limit analysis and certainly not as a linear elastic fracture mechanics solution. The incompatibility, which follows from the mixed mode solution, can be shown by calculating the displacements, which will show impossibilities and no continuity. The compatibility of the exact (mixed mode) solution of §4, is confirmed in the past [5] by calculation of displacements.

For pure mode I loading *p*, perpendicular to the crack, when shear stress $s = 0$, the equations (6.19) to (6.21), in *p*, apply. For pure mode II shear loading along the crack, when mode I tensile stress loading $p = 0$, the confocal coordinate equations (6.26) to (6.28) in *S* apply.

In appendix 2 of textbook [8], the following, still applied, equations of Williams [16], are given for pure mode I, p_1, when the shear stress loading $s_1 = 0$:

$$\sigma_{rr} = \left(1/4\sqrt{r}\right)\left[\, p_1\left\{-5\cos\left(\theta/2\right)+\cos\left(3\theta/2\right)\right\}\right] \tag{6.29}$$

$$\sigma_{\theta\theta} = \left(1/4\sqrt{r}\right)\left[\, p_1\left\{-3\cos\left(\theta/2\right)-\cos\left(3\theta/2\right)\right\}\right] \tag{6.30}$$

$$\tau_{r\theta} = \left(1/4\sqrt{r}\right)\left[\, p_1\left\{-\sin\left(\theta/2\right)-\sin\left(3\theta/2\right)\right\}\right] \tag{6.31}$$

and for pure mode II, when $p_1 = 0$:

$$\sigma_{rr} = \left(1/4\sqrt{r}\right)\left[\, s_1\left\{-5\sin\left(\theta/2\right)+3\sin\left(3\theta/2\right)\right\}\right] \tag{6.32}$$

$$\sigma_{\theta\theta} = \left(1/4\sqrt{r}\right)\left[\, s_1\left\{-3\sin\left(\theta/2\right)-3\sin\left(3\theta/2\right)\right\}\right] \tag{6.33}$$

$$\tau_{r\theta} = \left(1/4\sqrt{r}\right)\left[\, s_1\left\{\cos\left(\theta/2\right)+3\cos\left(3\theta/2\right)\right\}\right] \tag{6.34}$$

Using the properties:

$$\sin\left(3z\right) = 3\sin\left(z\right)-4\sin^3\left(z\right) \quad \rightarrow \quad \sin^3\left(z\right) = \left(3/4\right)\sin\left(z\right)-\left(1/4\right)\sin\left(3z\right)$$

$$\cos\left(3z\right) = -3\cos\left(z\right)+4\cos^3\left(z\right) \quad \rightarrow \quad \cos^3\left(z\right) = \left(3/4\right)\cos\left(z\right)+\left(1/4\right)\cos\left(3z\right)$$

equation (6.26) for pure shear loading *s* becomes:

$$\sigma_r = s\sqrt{c/2r}\cdot\sin\left(\theta/2\right)\cdot\left(1-3\sin^2\left(\theta/2\right)\right) = s\sqrt{c/2r}\cdot\left[\sin\left(\theta/2\right)-3\sin^3\left(\theta/2\right)\right] =$$

$$= s\sqrt{c/2r}\cdot\left[\sin\left(\theta/2\right)-3\left\{\left(3/4\right)\sin\left(\theta/2\right)-\left(1/4\right)\sin\left(3\theta/2\right)\right\}\right] =$$

$$= s\sqrt{c/2r}\cdot\left[-\left(5/4\right)\sin\left(\theta/2\right)+\left(3/4\right)\sin\left(3\theta/2\right)\right]$$

which is identical to the prescribed textbook [8] equation (6.32):

$$\sigma_{rr} = \left(1/4\sqrt{r}\right)\left[\, s_1\left\{-5\sin\left(\theta/2\right)+3\sin\left(3\theta/2\right)\right\}\right],$$

when: $s_1 = s\sqrt{(c/2)}$. The same also follows for eq.(6.27):

$$\sigma_\theta = -3s\sqrt{c/2r}\cdot\sin\left(\theta/2\right)\cdot\cos^2\left(\theta/2\right) \;= -3s\sqrt{c/2r}\cdot\sin\left(\theta/2\right)\cdot\left[1-\sin^2\left(\theta/2\right)\right] =$$
$$= -3s\sqrt{c/2r}\cdot\left[\sin\left(\theta/2\right)-\sin^3\left(\theta/2\right)\right] =$$
$$= -3s\sqrt{c/2r}\cdot\left[\sin\left(\theta/2\right)-\left\{(3/4)\sin\left(\theta/2\right)-(1/4)\sin\left(3\theta/2\right)\right\}\right] =$$
$$= -(3/4)s\sqrt{c/2r}\left[\sin\left(\theta/2\right)+\sin\left(3\theta/2\right)\right]$$

which is, again with: $s_1 = s\sqrt{(c/2)}$, identical to the prescribed textbook equation (6.33):

$$\sigma_{\theta\theta} = \left(1/4\sqrt{r}\right)\left[\, s_1\left\{-3\sin\left(\theta/2\right)-3\sin\left(3\theta/2\right)\right\}\right]$$

This same applies for: equation (6.28),

$$\tau_{r\theta} = s\sqrt{c/2r}\cdot\cos\left(\theta/2\right)\cdot\left(3\cos^2\left(\theta/2\right)-2\right) \;= s\sqrt{c/2r}\cdot\left(3\cos^3\left(\theta/2\right)-2\cos\left(\theta/2\right)\right) =$$
$$= s\sqrt{c/2r}\cdot\left((3/4)\cos\left(3\theta/2\right)+(9/4)\cos\left(\theta/2\right)-2\cos\left(\theta/2\right)\right) =$$
$$= (s/4)\sqrt{c/2r}\cdot\left(3\cos\left(3\theta/2\right)+\cos\left(\theta/2\right)\right)$$

which is, again with: $s_1 = s\sqrt{(c/2)}$, identical to the prescribed textbook equation: (6.34):

$$\tau_{r\theta} = \left(1/4\sqrt{r}\right)\left[\, s_1\left\{\cos\left(\theta/2\right)+3\cos\left(3\theta/2\right)\right\}\right]$$

The same can be done for the equations for pure mode I loading, e.g. equation (6.19):

$$\sigma_r = p\sqrt{c/2r}\cdot\cos\left(\theta/2\right)\cdot\left(1+\sin^2\left(\theta/2\right)\right) =$$
$$= p\sqrt{c/2r}\cdot\cos\left(\theta/2\right)\cdot\left(1+1-\cos^2\left(\theta/2\right)\right) = p\sqrt{c/2r}\cdot\left(2\cos\left(\theta/2\right)-\cos^3\left(\theta/2\right)\right) =$$
$$= p\sqrt{c/2r}\cdot\left(2\cos\left(\theta/2\right)-\left\{(1/4)\cos\left(3\theta/2\right)+(3/4)\cos\left(\theta/2\right)\right\}\right) =$$
$$= p\sqrt{c/2r}\cdot\left((5/4)\cos\left(\theta/2\right)-(1/4)\cos\left(3\theta/2\right)\right) = (p/4)\sqrt{c/2r}\cdot\left(5\cos\left(\theta/2\right)-\cos\left(3\theta/2\right)\right)$$

which is (6.29) and can be done for: eq.(6.20):

$$\sigma_\theta = p\sqrt{c/2r}\cdot\cos^3\left(\theta/2\right) = (p/4)\sqrt{c/2r}\cdot\left[\cos\left(3\theta/2\right)+3\cos\left(\theta/2\right)\right] \qquad = \text{(6.30)}$$

which is (6.30) and what also can be done for: eq.(6.21), which is identical to eq.(6.31):

$$\tau_{r\theta} = p\sqrt{c/2r}\cdot\cos^2\left(\theta/2\right)\sin\left(\theta/2\right) =$$
$$= p\sqrt{c/2r}\cdot\left(1-\sin^2\left(\theta/2\right)\right)\sin\left(\theta/2\right) = p\sqrt{c/2r}\cdot\left\{\sin\left(\theta/2\right)-\sin^3\left(\theta/2\right)\right\} =$$
$$= (p/4)\sqrt{c/2r}\cdot\left[4\sin\left(\theta/2\right)-\left\{3\sin\left(\theta/2\right)-\sin\left(3\theta/2\right)\right\}\right] = (p/4)\sqrt{c/2r}\cdot\left[\sin\left(\theta/2\right)+\sin\left(3\theta/2\right)\right]$$

Thus the general applied equations of [16], for pure mode I and pure mode II, which are identical to the confocal coordinate transformations of the exact elliptical coordinate equations, based on [6], published now in [5], chapter 8 and § 10.9), are given as mixed mode equations (6.35) to (6.37) in the textbooks:

$$\sigma_{rr} = \left(1/4\sqrt{r}\right)[\,p_1\left\{-5\cos\left(\theta/2\right)+\cos\left(3\theta/2\right)\right\}+s_1\left\{-5\sin\left(\theta/2\right)+3\sin\left(3\theta/2\right)\right\}] \tag{6.35}$$

$$\sigma_{\theta\theta} = \left(1/4\sqrt{r}\right)[\,p_1\left\{-3\cos\left(\theta/2\right)-\cos\left(3\theta/2\right)\right\}+s_1\left\{-3\sin\left(\theta/2\right)-3\sin\left(3\theta/2\right)\right\}] \tag{6.36}$$

$$\tau_{r\theta} = \left(1/4\sqrt{r}\right)[\,p_1\left\{-\sin\left(\theta/2\right)-\sin\left(3\theta/2\right)\right\}+s_1\left\{\cos\left(\theta/2\right)+3\cos\left(3\theta/2\right)\right\}] \tag{6.37}$$

although terms with p_1 only apply when $s_1 = 0$ and terms with s_1 only apply when $p_1 = 0$. Probably to hide the small variable origin of the equations, given in § 6.1, showing $r << c$, the replacements: $p_1 = p\sqrt{(c/2)}$, and $s_1 = s\sqrt{(c/2)}$ are made, what is against dimensional rules and transformation equations eq.(6.5) and eq.(6.6). Thus first c is omitted, by the shortcuts p_1, s_1, for $p\sqrt{(c/2)}$ and $s\sqrt{(c/2)}$ in order to escape the necessity $r << c$ and later c is again introduced as stress intensity what is based on dimensional analysis rules, with now the suggestion that it therefore is possible to apply $r >> c$. This close to cheating is of course not right. For dimensional reasons it is also not allowed to omit c from the copied equations at the start. This also applies for the stress function. Following the textbook derivation, the associated compatibility equation and stress equations are found by the most simple integration:

$$\nabla^2\left(\sigma_{rr}+\sigma_{\theta\theta}\right)=0 \rightarrow\ \nabla^2\nabla^2\Phi=0\ \ \rightarrow \tag{6.38}$$

$$\sigma_{rr} = \frac{1}{r^2}\frac{\partial^2\Phi}{\partial\theta^2}+\frac{1}{r}\frac{\partial\Phi}{\partial r} \tag{6.39}$$

$$\sigma_{\theta\theta} = \frac{\partial^2\Phi}{\partial r^2} = \left(3/4\right)r^{-1/2}F \tag{6.40}$$

$$\tau_{r\theta} = -\frac{\partial}{\partial r}\left(\frac{1}{r}\frac{\partial\Phi}{\partial\theta}\right) = -\frac{1}{r}\frac{\partial^2\Phi}{\partial r\partial\theta}+\frac{1}{r^2}\frac{\partial\Phi}{\partial\theta}\ = -\left(1/2\right)r^{-1/2}\frac{\partial F}{\partial\theta} \tag{6.41}$$

and the stress function is based on the copied $\sigma_{\theta\theta.}$ stress solution:

$$\Phi = r^{3/2}F\left(\theta\right) \tag{6.42}$$

because: $\Phi = (4/3)r^2\sigma_{\theta\theta.}$ (6.43)

Expressed in far field loading p_1 and s_1, the assumed stress function therefore is:

$$\Phi = r^{3/2}\left[\,p_1\left\{-\cos\left(\theta/2\right)-(1/3)\cos\left(3\theta/2\right)\right\}+s_1\left\{-\sin\left(\theta/2\right)-\sin\left(3\theta/2\right)\right\}\right] \tag{6.44}$$

In [10] also, in principle, the same form as eq.(6.42) is chosen for the stress function based on literally the same stress equations eq.(6.35) to (6.37) as in other textbooks, see e.g. [8]. The equations only apply at lower order distances from the crack-tip. Real occurring field stresses around the crack, which should be regarded, are given in Fig. 6.2.

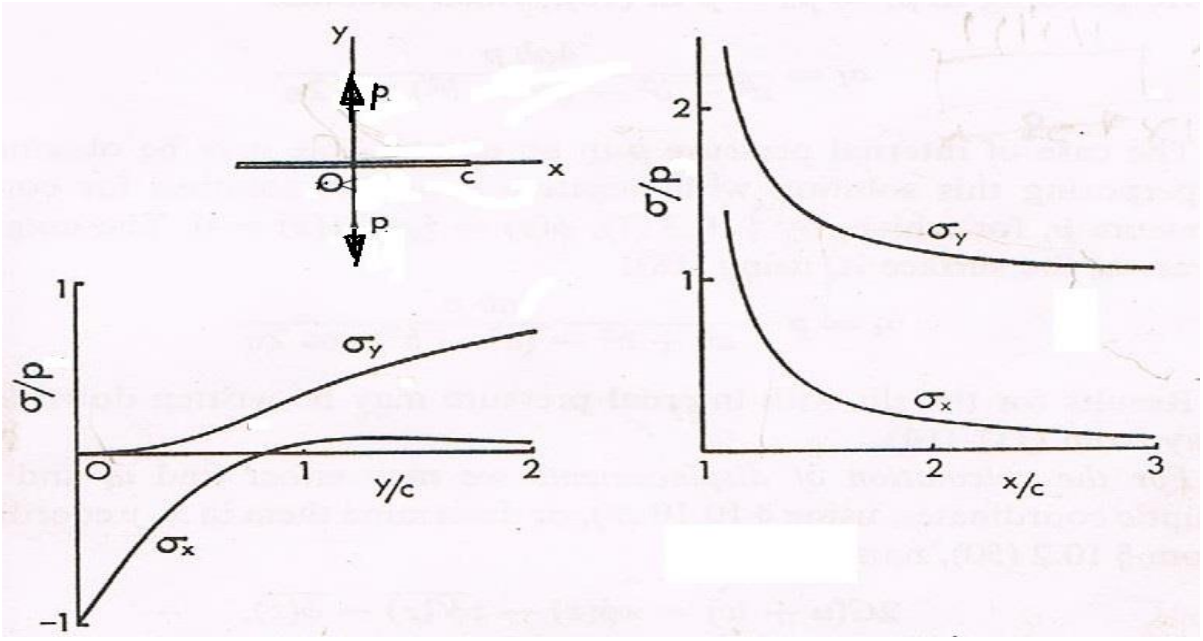

Fig. 6.2. Stresses for an elliptic flat crack [5] of length 2*c*, according to the solution of § 4.

The simple integration result, leads to the wrong textbook conclusion that stresses along the crack are zero. However, in eq.(6.35) to eq.(6.37) is σ_{rr} not zero at $\theta = \pi$, but, because the crack is empty, σ_{rr} has to be zero, just as $\tau_{r\theta}$, as boundary condition. Instead the tangential stress $\sigma_{\theta\theta}$ is zero, although this stress never is zero at any loading condition. For tension *p* perpendicular to the crack, the "bending" stress at the middle of the crack boundary is also *p* according to high-beam theory. See Fig. 6.2 of the exact solution. But the stress is maximal and even tends to infinite at the tip of a mathematical flat crack.. Clearly the simplified textbook approach is unacceptable mainly because *r* should be 2 orders smaller than the crack length 2*c* while it also is applied for much higher distances than the crack length. This has to be corrected to the common variable approach in line with § 4. Also the arbitrary extension in [8] of the stress equations with another constant stress at infinity (outside the stress function) and the applied stresses with positive power of *r*, thus infinite high "far field" stresses, are not allowed.

7. Linear elastic replacement of so-called non-linear fracture mechanics

7.1. Replacement of non-linear by linear reloading

Nonlinear fracture mechanic is empirical, based on the Ramberg-Osgood equation, which is a power law fitting curve of data. The line may represent any mathematical function which is adapted to follow the tangent direction of the line of the data. Chosen is some power

expression of *J* as energy release rate. The derivation and discussion of power law equations in general is e.g. given in [3]-§4.6, or extended in [17]-§2.5.2. For a right fracture application, a damage rate equation is necessary and in the power form, the power has the meaning of the activation volume parameter of the molecular Deformation Kinetics equation [2], which should be followed for the right approach to find the activation energy and entropy. Because not a critical energy release rate, but a critical stress intensity condition determines the ultimate load condition data should fit to eq.(7.1) which is given in Fig. 7.1, following [18]. The interpretation of this fracture strength data-line of geometrically similar specimens of Bazant, [18], was, to regard the inclined line, with a slope of - ½, to represent LEFM theory, the horizontal line to be the ultimate stress, strength theory and the curved, connecting line, to represent nonlinear fracture mechanics behavior, see e.g. [9]. However, there is no difference between nonlinear and linear elastic fracture mechanics data interpretation according to limit analysis. For both the linear elastic - full plastic approach of limit analysis should apply. The elastic - full- plastic boundary given in Fig. 2.2, exists as failure criterion, by a single curve in stress space which is given by Fig. 7.1. In this figure of e.g. [9], is d/d_o, the ratio of specimen size d, to the constant fracture process zone size d_o. But, because the line is the result of volume effect tests, the initial crack length is proportional to the test-specimen length. Thus, d/d_0, also can be regarded to be the ratio: initial open crack length, to the process zone size. The curved data line of Fig. 7.1, follows the equation:

$$\ln\sigma = \ln\sigma_0 - 0.5\ln\left(1 + d/d_0\right) \tag{7.1}$$

as result of a power law curve fitting. Eq.(7.1) therefore is:

$$\ln\left(\frac{\sigma}{\sigma_0}\right) = \ln\left(\frac{d_0 + d}{d_0}\right)^{-0.5} = \ln\left(\frac{d_0}{d_0 + d}\right)^{0.5} \quad \rightarrow \tag{7.2}$$

$$\rightarrow \sigma\sqrt{\pi\left(d_0 + d\right)} = \sigma_c\sqrt{\pi d_0} = K_c \tag{7.3}$$

in accordance with eq.(4.14). This confirms that the curve represents the stress intensity as ultimate state with K_c as critical stress intensity factor as should be for the linear state when $d/d_o >> 1$. For these higher values, the curved line approaches the drawn straight tangent line

$$\ln\sigma = \ln\sigma_0 - 0.5\cdot\ln\left(1 + d/d_0\right) = \ln\left(\sigma_0\right) - 0.5\ln\left(d'/d_0\right) \approx \ln\left(\sigma_0\right) - 0.5\ln\left(d/d_0\right) \tag{7.4}$$

with the necessary slope of the curve:

$$\frac{\partial\ln(\sigma/\sigma_0)}{\partial\ln(d/d_0)} \approx -0.5 \tag{7.5}$$

as limit. The real slope however is:

$$\frac{\partial \ln \sigma}{\partial \ln(d/d_0)} = \frac{\partial \ln(\sigma/\sigma_0)}{(d_0/d)\partial(d/d_0)} = \frac{d}{d_0}\frac{\partial\left(\ln(1+d/d_0)^{-0.5}\right)}{\partial(d/d_0)} = \frac{d}{d_0}\cdot\frac{-0.5}{1+d/d_0} = \frac{-0.5}{1+d_0/d} \tag{7.6}$$

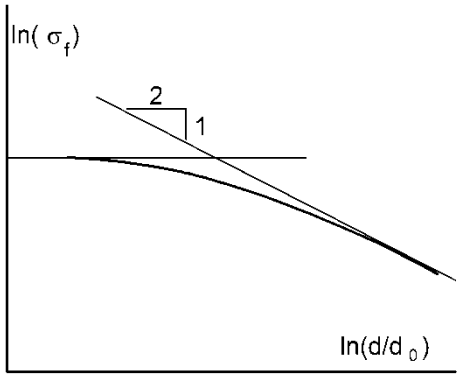

Figure 7.1. Limit LEFM behavior, depending on the crack-length *d* to process zone d_o ratio showing no nonlinearity. Thus a HRR-analog is not relevant. Data of Bazant [18].

This slope is: – 0.5 for $d >> d_o$ and this slope is zero when $d = 0$. Eq.(7.6) shows that for the whole curve LEFM applies and it is an indication that, at zero open crack dimensions, thus for: $d = 0$, the clear wood ultimate stress theory still follows LEFM, because it applies also for the constant initial length d_o (e.g. the constant fracture process zone length).
The derivation shows that for limit analysis extrapolation of linearity to the ultimate state, in accordance with the ultimate linear unloading – reloading behavior, the crack length, which is the focus distance of the elliptical first expanded of any crack form, is about equal to the open crack length for long sharp (flat) cracks, but is in general equal to: $d' = d + d_o$ thus equal to the open crack length plus the length d_o of the fracture process zone. Also in linear non-linear fracture mechanics this is applied.
After first yield drop, to half way unloading, maximal stress spreading is reached, and the strength theory further applies, according to [3], chapter 11, for further unloading by crack extension. Similar to steel, where yield drop is due to dislocation multiplication and dislocation breakaway, applies for wood, that the start of yield drop is due to micro-crack multiplication (e.g. as fracture process zone d_o) and micro- crack propagation and merging [3]. The, in § 4 derived, Wu-equation eq.(4.13), then reduces to eq.(4.14), expressed in stresses instead of in stress intensities and, with $\tau_u = 2\sigma_t$ for isotropic matrix stresses, turns to the failure criterion of strength theory for clear wood eq.(7.7), when total stresses, including the reinforcement, are accounted.

$$1 = \frac{\sigma_y}{\sigma_t} + \frac{\tau_{xy}^2}{\tau_u^2} \tag{7.7}$$

It thus follows, that the general accepted application of the nonlinear fracture mechanics models, to explain eq.(7.4), don't hold. The critical stress intensity only, is determining. Thus the ultimate tangential tensile strength of the crack boundary at the focus-crack boundary distance: $r = r_o$, is in all cases determining.

The application of geometrically similar specimens shows that there is no volume effect of the strength when sharp cracks are determining for failure because the same volume of the fracture process zone is determining. The proof and derivation of this and a wider and a total beam volume effect is derived in [3] at the discussion of the strength of wide angle notched beams.

7.2 Replacement of the large scale yielding J-R curve by LEFM critical stress intensity

It is not true, that total fracture always is instable, as is regarded for wood in textbooks e.g. in [8], or [9]. When the testing equipment with specimen is stiff enough, instable equilibrium is possible, making it possible to measure yield drop, the unloading behavior over the top of the loading curve. This unloading range, called "Griffith locus" [5] gives necessary information about the fracture processes in the ligament [3]. This behavior can be explained by void formation and void coalescence and necking action between remaining voids increasing the local strength by the stress spreading effect with hydrostatic stress formation as explained by "slip"-line theory [3]. In [19] this yield drop is extensively measured for wood. This explanation of the unloading behavior leads to a new theory of small crack extension with crack merging and stress spreading effect, [12], [3]. Figure 7.2 shows early instability and thus no yield drop. All tests of all series did show fracture at 2 mm crack extension, indicating instability of the test equipment at that point. The curved part of the loading line of Fig. 7.1 and 7.2, need not to mean influence of plastic flow. Here it is explained by LEFM as small crack propagation. Figure 7.2, given in [8], is regarded to be an example of so called, large scale yielding, where presence of excessive plasticity is assumed and where *K*, *J* or CTOD, are assumed to also depend on size and geometry of the test specimen. However this last plays no role in this case because identical test specimens are used in all tests of Fig. 7.2 and the, in this case necessary applied J_D, the deformation *J*, has the form:

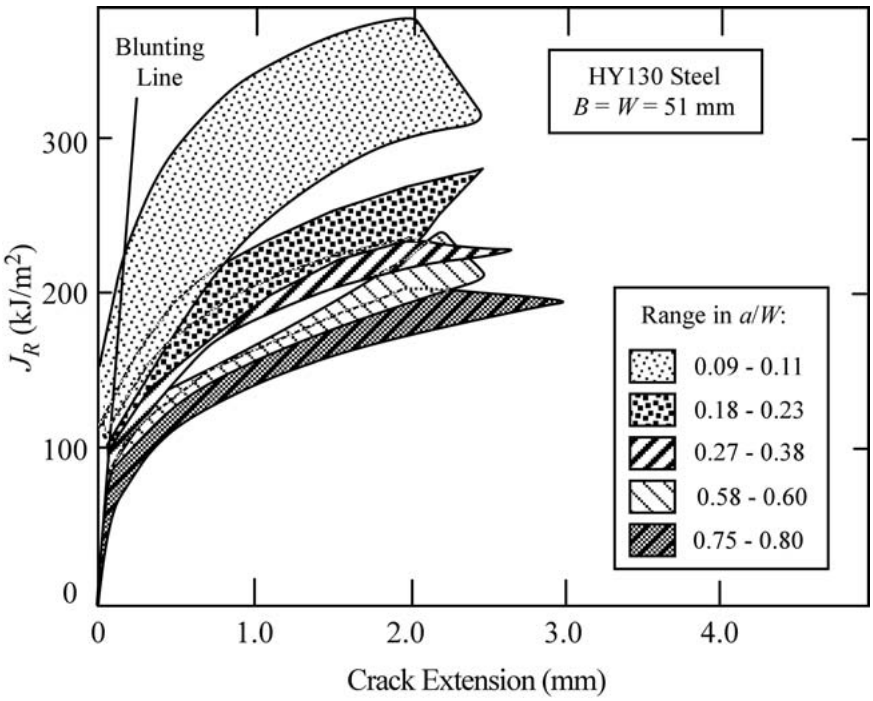

FIGURE 7.2 J_R in kN/m
Effect of crack length/specimen width ratio on *J-R* curves for HY130 steel single-edge-notched bend (SE(B)) specimens. Taken from Towers, O.L. and Garwood, S.J., ''Influence of Crack Depth on Resistance Curves for Three-Point Bend Specimens in HY130.'' ASTM STP 905, American Society for Testing and Materials, Philadelphia, PA, 1986, pp. 454–484.

$$J_D = 0.73\sigma_0 b\Omega = 0.73\sigma W\Omega \tag{7.8}$$

[8], where W and Ω are the same in all tests and where the actual stress on the ligament length b is replaced by the nominal stress on width W. The contour integral along the crack tip boundary is, at plastic deformation, given as:

$$J = \int_0^{\delta} \sigma_{yy} d\delta = \sigma_{ys}\delta \tag{7.9}$$

which is the comparable with equation of the crack tip opening displacement model, applied for small scale yielding and the linear elastic case.

$$J = m\sigma_u\delta \tag{7.10}$$

In this equation, m is a constant, which is the same for all series of same test specimens of Fig. 7.2, σ_u is the strength, and δ is the crack opening displacement, which also can be regarded the same at fracture for the series, because all specimens did show the same crack extension of 2 mm, when loaded from zero to the failure state and thus should show the same crack opening displacement over this equal range. It thus is probable that the ordinate *J*-values, at the abscissa at 2.0 mm crack extension, are proportional to the σ_u values according to eq.(7.10). All initial crack lengths are increased by 2 mm at failure. Thus a/W is increased

Table 2. – Critical stress intensity at supposed large scale yielding

Crack lengrh a/W				Stress and stress intensity	
group	mean	added	total	stress	reduced K_{Ic}
0.09 - 0.11	0.100	0.039	0.139	7.3 cm	$377.6 \cdot \sqrt{0.139} = 140.8$
0.18 - 0.23	0.205	"	0.244	5.2	$269.0 \cdot \sqrt{0.244} = 132.9$
0.27 - 0.38	0.325	"	0.364	4.6	$237.9 \cdot \sqrt{0.364} = 143.5$
0.58 - 0.60	0.590	"	0.629	4.4	$(227.6 \cdot \sqrt{0.629} = 180.5)$
0.75 - 0.80	0.775	"	0.814	4.0	$(206.9 \cdot \sqrt{0.814} = 186.7)$
					Mean critical: 139.1

by: 2/51= 0.039. Thus the final crack lengths and linear elastic stress intensities values of the series are given in Table 2. The ordinate σ_u values are measured in cm from Fig. 7.2. Under elastic, or so called small-scale yielding conditions, the critical stress intensity is:

$$K_{Ic} = \sigma\sqrt{\pi a} \tag{7.11}$$

where σ, the critical stress at the fracture site, and a, half of the critical crack length.

The mean value of the upper 3 series is 139.1, what has to be multiplied by $\sqrt{(\pi W)/\delta}$ to get the stress intensity. The higher stress intensity ratios of the last 2 series, indicate an overestimation due to overcritical initial crack lengths. According to the stress merging mechanism of [3] is for long cracks, the local ultimate stress (4.0 and 4.4 of Table 2) determining and not the stress intensity.

The very high variability of the strengths of the shortest initial crack lengths of $a/W = 0.1$ is due to absence of a pronounced ligament, so that small crack initiation ahead of the crack tip will be situated randomly and not at, and in line with, a ligament at the start.

Because nonlinear fracture mechanics, by an inconsistent J-integral, could not explain failure behavior given by Fig. 7.2 and, because always slip-line solutions are possible, it was concluded that excessive overall flow was determining for failure, regarded as: "large scale yielding". However, for the longer cracks, there is no indication of supposed excessive plastic flow (determining the ultimate state instead of local fracture) and apparent linear elastic limit

analysis approach is shown to be determining and to give one value of the critical stress intensity for all test-specimens with a sub-critical initial crack length.

8. Conclusions

- Outer the crack "boundary value analysis" of § 4, along the whole crack length, which delivers the exact mixed mode failure criterion, there exist a "crack tip" boundary value solution, discussed in § 6.1, which in modified form, is applied by all Textbooks. Both approaches appear to be based on the same Airy stress function solution of Stevenson. The derivation of the crack tip solution is based on small values of the elliptic variables ξ, η, what applies close to the crack tip. It is shown that this also applies for θ of Fig. 6.1. Because $\sqrt{(r/2c)}$ is small, also $\theta/2$ is small. This is due to the neglection of the first order terms of the solution with respect to terms containing the factor $\sqrt{(c/r)}$. This means that $\sqrt{(2c/r)}$ is one order higher than 1, or the maximal value of distance r of the focus to the crack boundary is 2 orders smaller than the crack length $2c$. However, the equations are wrongly applied for any value of r and θ, even for r > 2c and $\theta \neq 0$, giving distorted, and therefore impossible, results. For instance, the anti-symmetry stress condition at pure shear loading of the crack, is lost. This effect is diminished by ignoring the kink δ, of the elliptic boundary, thus taking the upper $\delta = 0$ in Fig. 6.1. This, however, only is right for mode I failure at $\theta = 0$, by a load at $\beta = \pi/2$. Thus by a tension load perpendicular to the crack. showing the presence of the hydrostatic stress state at the crack tip, in accordance with the exact equations in elliptical coordinates of § 4. This does not apply for shear loading in that model. Thus the maximum value condition $d\sigma_t/d\eta = 0$ has no meaning for the "crack tip" boundary value analysis because the analysis only applies for $\theta = 0$. Thus for shear and mixed tension-shear modes, only the boundary value analysis along the whole crack length of § 4 applies. Thus as conclusion:

- The "crack tip" boundary value analysis of § 6 should not be applied anymore and revision of the mathematical equations of all textbooks is necessary following § 4 and [5].

- The proof is further given, in § 6.2, that these general accepted textbook equations, for pure shear loading and pure tension perpendicular to the crack plane, are literal copies of the equations of the "crack tip boundary value" analysis, for elliptical cracks, according to the Stevenson Airy stress solution. Instead of a mixed mode failure criterion, the textbooks solution wrongly consist of the sum of the solution for pure shear stress loading alone, with the solution for pure tensile stress loading perpendicular to the crack direction alone,

although these two solutions exclude each other and cannot apply and act at the same time. This delivers, a wrong, incompatible, system which does not satisfy the mixed mode failure criterion and the crack boundary conditions and therefore does not represent a linear elastic fracture mechanics solution. This has to be replaced by the derived mixed mode fracture criterion, eq.(5.8) for wood.

- The crack "boundary value" analysis of § 4, delivers the mixed I-II mode failure criterion, thus gives the critical load combinations of far field tension perpendicular to the crack and shear stress along the crack, for crack boundary failure, caused by local ultimate uniaxial tensile stress (apparent cohesion strength). This mixed mode failure criterion (for wood) gives the compatible ultimate tension - shear load combinations. It also gives the compatible uniaxial strength for tension without shear loading and ultimate shear strength without tensional loading. Failure by separate independently acting modes, as assumed by Textbooks, is not compatible thus does not exist.
- The critical stress intensity, as fracture criterion of wood and isotropic materials, depending on the initial crack length, is given by Fig. 7.1. There is no need to regard the curved part as plastic or non-linear elastic behavior (as is done) because the whole curve represents critical stress intensity, based on the critical linear elastic behavior, up to yield, of limit analysis.
- Equations in $1/r$ should be in $1/r_o$ to give the ultimate state, where r_o is the distance from the focus to the crack-tip. This is not applied in textbooks. High stresses means short cracks, as given in fig. 7.1. This thus also applies for the very small cracks of clear wood, what need not to indicate a plastic stage as assumed in Textbooks.
- The exact boundary value solution, of a flat elliptic crack in an infinite medium, based on complex potentials solution of the Airy stress function of Stevenson, is given in elliptic coordinates, providing easy stress boundary conditions along the whole flat elliptic crack boundary. The then right boundary value solution gives the mixed I-II mode fracture criterion (here for wood) which, when transformed to Cartesian coordinates, is a simple expression, eq.(4.13). This exact approach should be applied by the Textbooks.
- The energy approach of Griffith shows that a critical energy release rate or *J*-integral, as such, does not exist and thus is not determining for fracture. Necessary is a related critical stress intensity, which represents the critical state for failure. The applied, so called G-criterion, eq.(2.3), is not related to a stress intensity in its definition and thus is not right.
- As given by Fig. 2.1 and 2.2, the first loading to the ultimate state may cause plastic- and other non-linear deformation. On unloading and reloading the behavior has become perfect

linear elastic, which represents the linear elastic behavior up to yield of limit analysis. There is no need to know the first elastic- increasing plastic stage. Relevant is the lower bound linear elastic-full plastic approach of limit analysis only.

- It is important to notice that it is not needed to know when instable fracture occurs, because this is an instability of the testing devise and not a material property. Therefore, the R-curve need not to be postulated. As lower bound, only a save value at, or below, the top of the loading curve should be chosen as ultimate yield state.
- To avoid configurational changes, which would prevent a right application of limit analysis theorems, virtual work and virtual displacements should be applied and only first expanded of the load and displacements and the stress division, apply, because second and higher order quantities are zero in the virtual limit. For that reason, elementary beam theory applies for the compliance method of fracture mechanics (as is general accepted). Thus linear elastic loading behavior represents the accountable first expanded of any non-linear loading behavior and non-linear fracture mechanics has to be replaced by the linear elastic approach of limit analysis. This is applied in the Building codes.
- The J-integral from contour integration is path dependent in the common structural elastic plastic materials and tends to zero as the contour shrinks to the crack tip. This also applies for a growing crack in an elastic material. A critical energy release rate or J only exist when related to a critical stress intensity and thus does not represent a material property. Because not the deformation theory, but the flow theory of plasticity applies, for structural materials, no path-independence of *J* is possible and under real occurring load histories, which include local unloading, e.g. at (small) cracks extension, *J* has no physical meaning.
- Crack extension, by shear along the crack, or tension perpendicular to the crack or by a combination of both, occurs when the uniaxial tensile strength at the crack boundary is reached. The failure modes are not fracture modes but crack opening modes by elastic strain release. The crack “boundary value analysis” then delivers the mixed mode failure criterion eq.(4.13), which is empirically verified at a high significance (Table 1).
- At the smallest radius on top of the crack tip, high stress and strength is possible due to the occurring hydrostatic stress state. This is a consequence of the critical distortional energy principle of the strength where the shear stress is zero. An undetermined high strain and tensile strength then is possible. This hydrostatic stress state is shown to apply not only for pure tensile loading perpendicular to the crack, but as derived, also applies for pure shear loading along the crack. Thus therefore it applies for any load combination. Probably the

radius of the crack tip is able to be adapted to avoid strain differences, creating a zone of hydrostatic stresses (fracture process zone) above the crack tip in combination with a plastic zone extension. This is the explanation of the empirical found high hydrostatic stresses in the fracture process zone. .

- Hydrostatic stress failure is not determining for failure at the crack tip and thus is not part of the mixed mode failure criterion. Mixed mode tests in tension and shear, on short sawn notches, in clear wood, may show oblique crack extension according to ultimate uniaxial tensile stress failure at the crack tip boundary. This is confirmed by theory and by tests on the same notch form (not pre-cracked) in concrete. Further crack propagation was also normal to the maximal principal stress (confirmed by finite element calculation). The sawn notch had a rectangular top, thus is flat at the top with 2 wide angle (90^o) side notches at the crack boundary. This means, that at high stress (due to short cracks), and absence of small cracks near the crack tip, (clear wood) these wide angle notches may be determining. In common tests, this oblique crack extension does not occur, due to razor blade sharpening of the notch. This delivers a longer crack with smaller crack-tip-radius on top, what then always is determining, showing then the wanted collinear crack extension adjacent to the hydrostatic stress spot.

- The so called nonlinear fracture mechanics is not able to explain failure behavior as given by Fig. 7.2, because the J integral does not exist in this case and because always slip-line solutions are possible, it was concluded that excessive overall flow was determining for failure, what is called: “large scale yielding”. However, in limit analysis, any equilibrium system applies to obtain a lower bound solution, also applicable when there is no excessive plastic flow. Thus linear elastic-full plastic limit analysis approach is determining and gives one value of the critical stress intensity for all test-specimens with a sub-critical initial crack length (See Table 2).

- Based on the potentials eq.(4.3) and eq.(4.4) all stresses everywhere in the field around the crack can be calculated. See Fig. 6.2 for the result. And also the stress transformations are known. Because:

$$\sigma_\xi + \sigma_\eta = \sigma_x + \sigma_y = 2\left[\phi'(z) + \overline{\phi}'(z)\right] \tag{4.19}$$

$$\sigma_\eta - \sigma_\xi + 2i\tau_{\xi\eta} = (\sigma_y - \sigma_x + 2i\tau_{xy})e^{2i\delta} = 2[\overline{z}\phi''(z) + \psi'(z)][\omega'(\zeta)/\overline{\omega}'(\zeta)] \tag{4.20}$$

τ_{xy} is known from the imaginary part of eq.(4.20) and $\sigma_y - \sigma_x$ from the real part. Thus with eq.(4.19), all stresses are known in Cartesian coordinates. The same is possible for transformation to polar coordinates.

- The main error of non-linear fracture mechanics is the postulate of existence of critical energy release rates for each stress type, which consequently act independently of each other, and thus violate compatibility conditions and violate the necessary mixed mode fracture criterion. Important is that it is the consequence of that postulate, that no compatibility and no mixed mode failure criterion is possible.

- The exact equations (4.19 to 4.21) in elliptical coordinates, show, that for pure mode I and for pure shear loading along the crack length, a hydrostatic ultimate stress occurs at the crack tip. In the limit both, at the same place and at the magnitude. This therefore also applies for any load combination. According to the critical distortional energy principle this may provide an undetermined high strength to cover the high singularity stress,

- The presence of sharp cracks in materials thus indicate the presence of pure hydrostatic stress (without shear) and the presence of an isotropic matrix, showing behavior as reinforced material.

References

[1] van der Put TACM. A general failure criterion for wood. Proceed. 15th CIB IUFRO Timber Eng. Group Meeting, Boras, 1982, Sweden.

[2] van der Put TACM. Deformation and Damage Processes in Wood. Doct. thesis, Delft University Press 1989.

[3] van der Put TACM. A New Fracture Mechanics Theory of Wood, Extended second edition. Nova Science Publishers Inc. 2011; pp 247 x1

[4] van der Put TACM. Exact Stability Calculation of Timber beams and Columns, § 3 Open Constr Build Techn J 2013; 7: 20-32.

[5] Jaeger JC, Cook NGW, Zimmerman RW. Fundamentals of Rock Mechanics. Blackwell Publishing, 4th ed. 2007

[6] Stevenson A.C. (1945) Complex potentials in two-dimensional elasticity. Proc. Roy. Soc. London 1945; A184: 129-79.

[7] van der Put TACM. Breukcriterium voor beton als ondergrens van de sterkte bepaald volgens de evenwichtsmethode, Cement XXVI, 1974; nr.l0; p. 420-421 (in Dutch).

[8] Anderson TL. Fracture Mechanics, Fundamentals and applications CRC Press Taylor & Francis Group, third edition 2005 (as E-book available on internet).

[9] Smith I., Landis E, Gong M. Fracture and Fatigue in Wood. John Wiley & Sons Ltd. The Atrium 2003.

[10] Schreurs PJG. Fracture Mechanics, Lecture notes - course 4A780 Concept version 2012. Eindhoven University of Technology.

[11] Valentin GH, Boström L, Gustafsson PJ, Ranta-Maunus A, Gowda S. Application of fracture mechanics to timber structures. RILEM state-of-the-art report 1991.

[12] van der Put TACM. Derivation of the bearing strength perpendicular to the grain of locally loaded timber blocks, Holz Roh Werkst 2008; 66: 409–417.

[13] Mall S, Murphy JF, Shottafer JE. Criterion for Mixed Mode Fracture in Wood. J Eng Mech 1983; 109(3): 680-690.

[14] Wu EM. Application of fracture mechanics to anisotropic plates, ASME J Appl Mech Series E, 34 4, Dec. 1967, pp. 967-974..

[15] van der Put TACM. A continuum failure criterion applicable to wood, J Wood Sci 2009; 55:315–322.

[16] Williams ML. On the Stress Distribution at the Base of a Stationary Crack. J of Appl Mech, 1957; 24: pp. 109–114.

[17] van der Put TACM. B.2 Transformations of wood and wood-polymers. Delft Wood Science Foundation Publ. Series 2015 nr. 2-2 - ISSN 1871-675x

[18] Bazant ZP. (1999) Size effect on structural strength: a review. Archive of Applied Mechanics; 69: 703-725.

[19] Boström L. Method for determination of the softening behavior of wood and the applicability of a nonlinear fracture mechanics model. Doct. thesis, TVBM-1012, 1992.

Figures

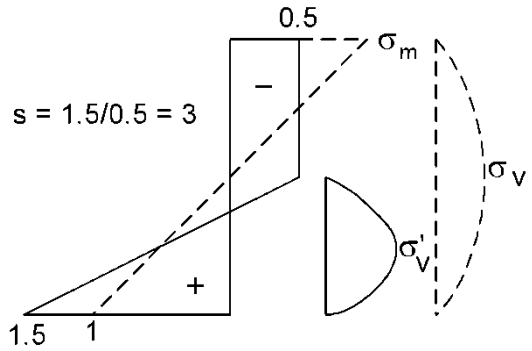

Figure 2.1. Bending stress diagram

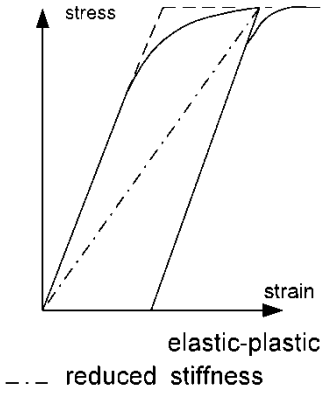

Figure 2.2. Elastic –full plastic behavior

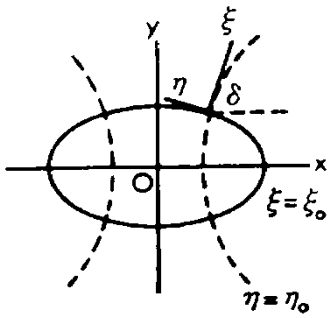

Figure 4.1. Elliptic hole and coordinates (van der Put 2011)

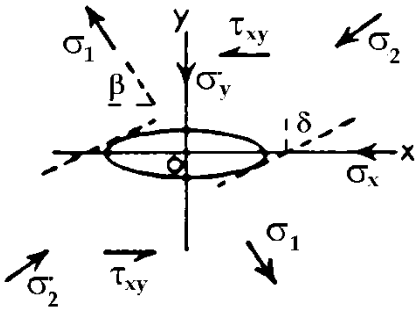

Figure 4.2. - Stresses in the notch plane Ox (van der Put 2011)

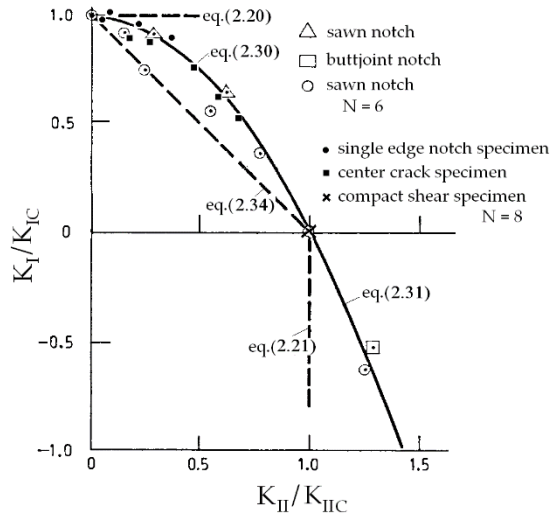

Figure 5.1. Equation numbers are of the first edition of (van der Put 2011)

Eq.(2.31) = (5.1); Eq.(2.30) = (4.13)

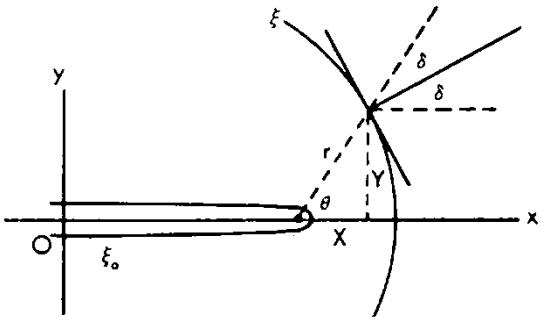

Figure 6.1. Confocal polar coordinates for transformation of the elliptical crack coordinates to polar crack tip coordinates

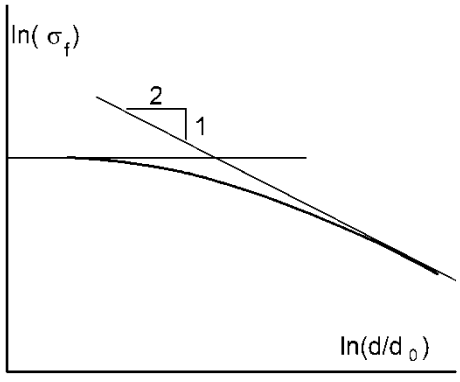

Figure 7.1. Limit LEFM behavior, depending on the crack-length *d* to process zone d_o ratio showing no nonlinearity. Thus a HRR-analog is not relevant. Data of (Bazant 1999).

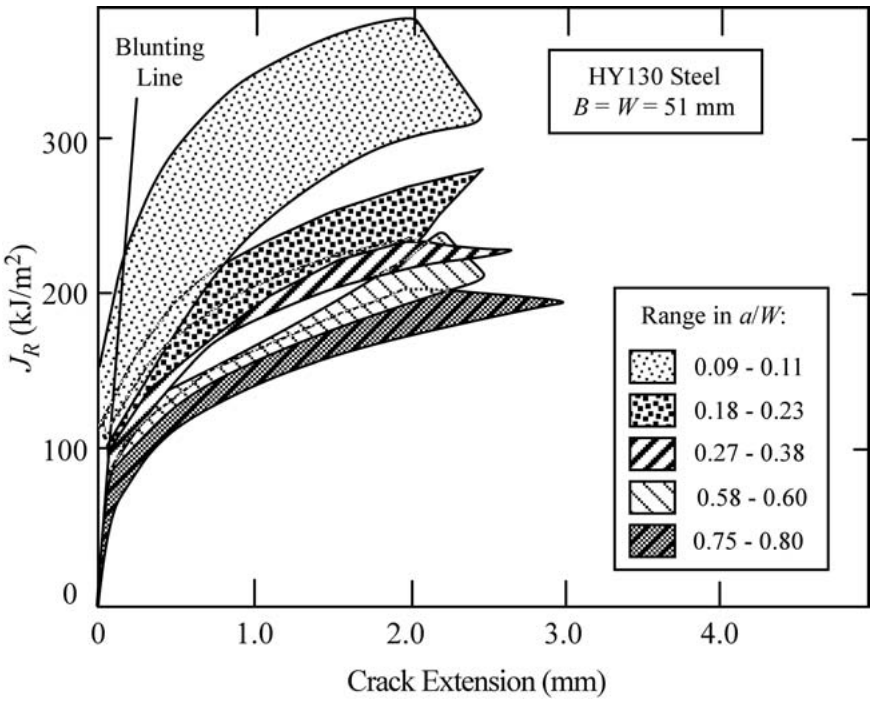

FIGURE 7.2 J_R in kN/m
Effect of crack length/specimen width ratio on *J-R* curves for HY130 steel single-edge-notched bend (SE(B)) specimens. Taken from Towers, O.L. and Garwood, S.J., ‘‘Influence of Crack Depth on Resistance Curves for Three-Point Bend Specimens in HY130.’’ ASTM STP 905, American Society for Testing and Materials, Philadelphia, PA, 1986, pp. 454–484.

Tables

Table 1. - Lack of fit values for supposed failure criteria (Mall et al 1983)

Failure criterion	*p*-value
$K_I / K_{Ic} = 1$	0.0001
$K_I / K_{Ic} + K_{II} / K_{IIc} = 1$	0.0001
$K_I / K_{Ic} + \left(K_{II} / K_{IIc}\right)^2 = 1$	0.5629
$\left(K_I / K_{Ic}\right)^2 + K_{II} / K_{IIc} = 1$	0.0784
$\left(K_I / K_{Ic}\right)^2 + \left(K_{II} / K_{IIc}\right)^2 = 1$	0.0001

Table 2. – Critical stress intensity at supposed large scale yielding

Crack length a/W				Stress and stress intensity	
group	mean	added	total	stress	reduced K_{Ic}
0.09 - 0.11	0.100	0.039	0.139	7.3 cm	$377.6 \cdot \sqrt{0.139} = 140.8$
0.18 - 0.23	0.205	"	0.244	5.2	$269.0 \cdot \sqrt{0.244} = 132.9$
0.27 - 0.38	0.325	"	0.364	4.6	$237.9 \cdot \sqrt{0.364} = 143.5$
0.58 - 0.60	0.590	"	0.629	4.4	$227.6 \cdot \sqrt{0.629} = 180.5$
0.75 - 0.80	0.775	"	0.814	4.0	$206.9 \cdot \sqrt{0.814} = 186.7$
					Mean critical: 139.1

Appendix x

D. Structural failure criteria of wood structures

Introduction

The developed exact theory is given in the appended publications denoted by D, thus: **D(1991)**, **D(2008a)**, **D(2008b)**, **D(2010)**, **D(2011)**, **D(2012a) D(2012b)** and primary, by the partly expired **D(2006a)**, **D(2006b).** Other relevant derivations and applications are mentioned in these publications. The theory in all appended publications was derived by T.A.C.M. van der Put as theory of perfect plasticity. Because a complete loading history analysis, with gradual increasing plasticity, until collapse is too extended and not necessary for ultimate state estimation, the relatively simple limit analysis method can always be applied instead. Then, no matter how complex the geometry of a problem, or loading condition, is, it is always possible to obtain a realistic value of the collapse load. This basic theory is discussed in the next section: D-1.

D-1. Upper and lower bound limit analysis of wood structures

The ultimate state represents a variational extremum problem and thus is based on small geometrical changes (using undeformed dimensions in the equilibrium equations). Because of the small changes, the virtual work equations apply. Because the top of a loading curve can be reached in many ways, differing an internal equilibrium system from each other, the previous loading history is not involved in the determination of the extremum and it is possible to use a linear- full plastic loading diagram for limit analysis (as is applied e.g. in exact fracture mechanics **C(2011b))**. In Fig.D-1, a scheme of the loading curve is given with

a boundary (the elastic limit, depending on loading rate, temperature, etc.) where below the behavior can be assumed to be elastic (especially after mechanical conditioning) and where above the gradual flow of components at peak stresses and micro-cracking may have a similar effect as plastic flow with a hardening history up to the ultimate failure stress. The total main plane loading curves due to flow, damage and hardening behavior at any deformation rate, temperature, moisture content, loading history etc., up to flow and failure, fully can be described by deformation kinetics (see Annex B). When this loading curve is followed to a chosen or real ultimate stress point and then unloaded, the elastic and "plastic" deformation is known of that limit point. (The "plastic" amount (permanent strain in Fig.D-1 depends on the past, unknown, loading history at growth, drying, manufacturing, transport and pre-testing).

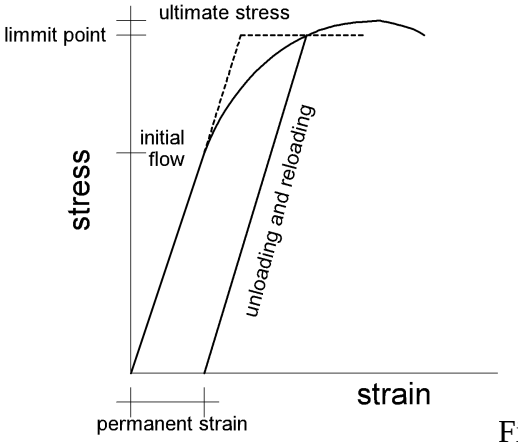

Fig.D-1. Loading curve

On reloading, the curve is elastic up to the limit point and it is possible to regard an elastic – full plastic description of the loading line according to the dashed line in Fig.D-1 as an allowable displacement field in the sense of limit analysis (that needs not to be the real occurring displacement for the virtual work equations). Also a reduced stiffness can be chosen as done for the Building Codes.

The virtual work equation, represents the extremum condition that the first variation of the potential energy is zero. Thus a small variation of the total potential energy vanishes when the structure is in equilibrium. Thus the total work of an equilibrium system is zero for any virtual displacement. The virtual work equation thus is based on an equilibrium set and a compatible set, which need not, and should not, be related. Thus:

$$\int_A T_i \dot{u}_i^* dA + \int_V F_i \dot{u}_i^* dV = \int_V \sigma_{ij} \dot{\varepsilon}_{ij}^* dV \,, \qquad \text{(D-1)}$$

integrated over the whole area *A* and volume *V* of the body. T_i and F_i are external forces on surface and in the body; σ_{ij} are the stresses, in equilibrium with the external forces, which need not to be the real actual occurring stresses. The asterisk is used for the compatible set, to emphasize that the two sets are not related, thus are completely independent.

A valid equilibrium set must satisfy the equilibrium equations:

$$\frac{\partial \sigma_{ji}}{\partial x_j} + F_i = 0 \qquad \text{(D-2)}$$

and the equilibrium conditions at the load applications points (as boundary condition).

Of the compatible set, are the strains $\dot{\varepsilon}_{ij}^*$ compatible with real or imagined (virtual) displacement rate $\dot{u}_i^*$ of the points of application of the external forces, following the strain

and displacement rate compatibility equation.

$$2\dot{\varepsilon}_{ij}^{*} = \frac{\partial \dot{u}_i^{*}}{\partial x_j} + \frac{\partial \dot{u}_j^{*}}{\partial x_i} \tag{D-3}$$

Virtual displacements are not real, they can be physically impossible but they must be compatible with the geometry of the original structure and they must be small enough so that the original geometry is not significantly altered.
As equilibrium set, also the load increments can be used giving the rate equation:

$$\int_A \dot{T}_i \dot{u}_i^{*} dA + \int_V \dot{F}_i \dot{u}_i^{*} dV = \int_V \dot{\sigma}_{ij} \dot{\varepsilon}_{ij}^{*} dV \,. \tag{D-4}$$

In the linear-full plastic schematization is the plastic zone a line in Fig.D-2, but is a plane in stress space. Plastic flow occurs when the yield function $f\left(\sigma_{ij}\right) = 0$ is satisfied. It is necessary that:

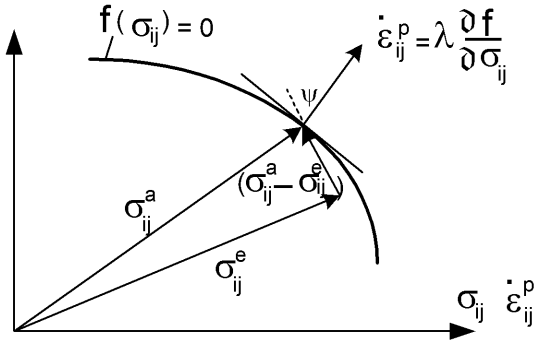

Fig.D-2 Yield surface and flow rule

$$\left(\sigma_{ij}^{a} - \sigma_{ij}^{c}\right) \cdot \dot{\varepsilon}_{ij}^{p} \geq 0 \,, \tag{D-5}$$

Thus this dot product is always positive and shows an angle $\psi \leq 90^{0}$, because thermo-dynamical real work (and real dissipation) has to be positive. Eq.(D-5) only is for all cases fulfilled when the vector $\dot{\varepsilon}_{ij}^{p}$ is perpendicular to the curve $f\left(\sigma_{ij}\right) = 0$, thus is in the direction of $\partial f / \partial \sigma_{ij}$. This is the convexity requirement or normality rule wherefore the principle of maximal local energy dissipation applies for the actual stress state, i.e. the projection in fig.D-2, of vector σ_{ij}^{a} on $\dot{\varepsilon}_{ij}^{p}$ is then maximal, higher than such projection of any other critical vector. In that case also the zero value of eq.(D-5) is reached for the plastic stress increment. Thus for the plastic flow increment then is:

$$\dot{\sigma}_{ij} \cdot \dot{\varepsilon}_{ij}^{p} = 0 \tag{D-6}$$

From eq.(D-4) and (D-6) follows, that when the limit load is reached and the deformation proceeds under constant load, all stresses remain constant and only plastic, (not elastic) increments of strain occur. Because at collapse, eq.(D-4) becomes:

$$\int_A \dot{T}_i^{c} \dot{u}_i^{c} dA + \int_V \dot{F}_i^{c} \dot{u}_i^{c} dV = \int_V \dot{\sigma}_{ij}^{c} \dot{\varepsilon}_{ij}^{c} dV \,. \tag{D-7}$$

With $\dot{T}_i^{c} = \dot{F}_i^{c} = 0$, and with elastic and plastic parts of strain, $\dot{\varepsilon}_{ij}^{c} = \dot{\varepsilon}_{ij}^{ec} + \dot{\varepsilon}_{ij}^{pc}$ is eq.(D-7):

$$\int_V \dot{\sigma}_{ij}^{c} \dot{\varepsilon}_{ij}^{c} dV = \int_V \dot{\sigma}_{ij}^{c} (\dot{\varepsilon}_{ij}^{ec} + \dot{\varepsilon}_{ij}^{pc}) dV = \int_V \dot{\sigma}_{ij}^{c} (\dot{\varepsilon}_{ij}^{ec}) dV = 0 \tag{D-8}$$

because of eq.(D-6), and thus $\dot{\sigma}_{ij}^{c} \dot{\varepsilon}_{ij}^{ec} = 0$. Thus the elastic strain increment and consequently,

the elastic stress increment, are zero and all deformation is plastic. Thus the elastic characteristic plays no part in the collapse at the limit load.
Next it is possible to give the proof of the lower and upper bound theorems of limit analysis. The lower bound theorem states that, if an equilibrium distribution of stress σ_{ij}^{E}, covering the whole body, can be found, which balances the applied loads and is everywhere below yield $f\left(\sigma_{ij}^{E}\right)<0$, then the body will not collapse.
To prove this, assume that it is false, then two collapse equations exist:

$$\int_A T_i^c \dot{u}_i^c dA + \int_V F_i^c \dot{u}_i^c dV = \int_V \sigma_{ij}^c \dot{\varepsilon}_{ij}^c dV$$

$$\int_A T_i^c \dot{u}_i^c dA + \int_V F_i^c \dot{u}_i^c dV = \int_V \sigma_{ij}^E \dot{\varepsilon}_{ij}^c dV$$

and consequently is, because all deformation is plastic:

$$\int_V (\sigma_{ij}^c - \sigma_{ij}^E)\dot{\varepsilon}_{ij}^{pc} dV = 0, \qquad \text{(D-9)}$$

and because according to eq.(D-5): $(\sigma_{ij}^c - \sigma_{ij}^E)\dot{\varepsilon}_{ij}^{pc} > 0$ for σ_{ij}^E below yield, eq.(D-9) cannot be true and the lower bound theorem is proved.
The upper bound criterion states that if a compatible mechanism of plastic deformation is found, which satisfies the displacement boundary conditions, then the loads, determined by equating the rate, at which the external forces do work, eq.(D-10):

$$\int_A T_i \dot{u}_i^{p^*} dA + \int_V F_i \dot{u}_i^{p^*} dV, \qquad \text{(D-10)}$$

to the rate of internal dissipation, eq.(D-11):

$$\int_V D(\dot{\varepsilon}_{ij}^{p^*}) dV = \int_V \sigma_{ij}^p \dot{\varepsilon}_{ij}^{p^*} dV \qquad \text{(D-11)}$$

will be either higher or equal to the actual limit load.
Again, assume the theorem false, and the computed loads to be less than the actual limit load, then the following equation should apply:

$$\int_A T_i \dot{u}_i^{p^*} dA + \int_V F_i \dot{u}_i^{p^*} dV = \int_V \sigma_{ij}^E \dot{\varepsilon}_{ij}^{p^*} dV \qquad \text{(D-12)}$$

with σ_{ij}^E everywhere below yield. Because T_i and F_i follow from equating eq.(D-10) and eq.(11), it follows that:

$$\int_V (\sigma_{ij}^{p^*} - \sigma_{ij}^E)\dot{\varepsilon}_{ij}^{p^*} dV = 0 \qquad \text{(D-13)}$$

However, according to eq.(D-5) $(\sigma_{ij}^{p^*} - \sigma_{ij}^E)\dot{\varepsilon}_{ij}^{p^*} > 0$ for σ_{ij}^E below yield, what leads to a contradiction and thus to the proof of the upper bound theorem.
Some corollaries, to be mentioned, following from the lower bound theorem, are, that:
- Initial stress or deformation have no effect on the plastic limit or collapse load provided the geometry is essential unaltered. This is e.g. applied in **C(2014)**.
- The limit load, computed from a convex yield surface, which circumscribes the actual surface, will be an upper bound on the actual limit load. The limit load computed from an inscribed surface will be a lower bound of the actual collapse load. This last is applied in the derivations of e.g. **D(2008a)**, by using the, in the von Mises inscribed Tresca polynomial).
The graphical proof of the lower and upper bound is as follows:
In fig.D-3 is the plastic strain increment $\dot{\varepsilon}_c$ normal to the failure surface and is vector σ_l just inside the surface. Index *c* stands for actual collapse load and index *l* indicates lower bound.

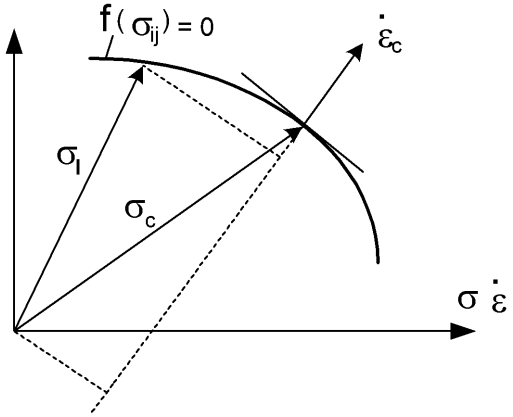

Fig.D-3. Proof of the lower bound theorem

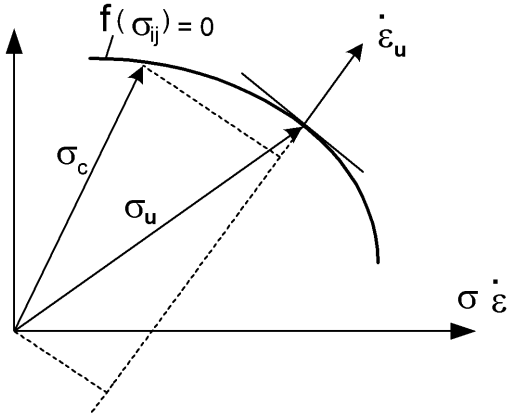

Fig.D-4. Proof of the upper bound theorem

According to the virtual work principle is for collapse:

$$\sum F_c \dot{w}_c = \int_V \sigma_c \dot{\varepsilon}_c dV$$

and for a lower bound:

$$\sum F_l \dot{w}_c = \int_V \sigma_l \dot{\varepsilon}_c dV$$

where *F* is the external force and *w* the displacement of *F*. The internal stress is σ_c with $\dot{\varepsilon}$ as strain increment. The dot product is the product of the strain increment with the components of the stress vector in the direction of strain increment. According to fig.D-3 is

$$\sigma_l \dot{\varepsilon}_c \le \sigma_c \dot{\varepsilon}_c$$

thus is a lower bound due to the convexity of the yield function.
For the proof of the upper bound criterion applies, according to fig.D-4, that collapse must have occurred if:

$$\sum F_u \dot{w}_u = \int_V \sigma_u \dot{\varepsilon}_u dV$$

According to the virtual work equation is: the upper bound criterion

$$\sum F_c \dot{w}_u = \int_V \sigma_c \dot{\varepsilon}_u dV$$

The figure shows by projection of σ_u and σ_c on $\dot{\varepsilon}_u$ that:

$\sigma_u \dot{\varepsilon}_u \geq \sigma_c \dot{\varepsilon}_u$

Thus also $F_u \geq F_c$ and F_u thus is the upper bound because of the convexity of the yield function.

D. Structural failure criteria of wood structures

Introduction

The developed exact theory is given in the appended publications denoted by D, thus: **D(1991)**, **D(2008a)**, **D(2008b)**, **D(2010)**, **D(2011)**, **D(2012a) D(2012b)** and primary, by the partly expired **D(2006a)**, **D(2006b).** Other relevant derivations and applications are mentioned in these publications. The theory in all appended publications was derived by T.A.C.M. van der Put as theory of perfect plasticity. Because a complete loading history analysis, with gradual increasing plasticity, until collapse is too extended and not necessary for ultimate state estimation, the relatively simple limit analysis method can always be applied instead. Then, no matter how complex the geometry of a problem, or loading condition, is, it is always possible to obtain a realistic value of the collapse load. This basic theory is discussed in the next section: D-1.

D-1. Upper and lower bound limit analysis of wood structures

The ultimate state represents a variational extremum problem and thus is based on small geometrical changes (using undeformed dimensions in the equilibrium equations). Because of the small changes, the virtual work equations apply. Because the top of a loading curve can be reached in many ways, differing an internal equilibrium system from each other, the previous loading history is not involved in the determination of the extremum and it is possible to use a linear- full plastic loading diagram for limit analysis (as is applied e.g. in exact fracture mechanics **C(2011b))**. In Fig.D-1, a scheme of the loading curve is given with a boundary (the elastic limit, depending on loading rate, temperature, etc.) where below the behavior can be assumed to be elastic (especially after mechanical conditioning) and where above the gradual flow of components at peak stresses and micro-cracking may have a similar effect as plastic flow with a hardening history up to the ultimate failure stress. The total main plane loading curves due to flow, damage and hardening behavior at any deformation rate, temperature, moisture content, loading history etc., up to flow and failure, fully can be described by deformation kinetics (see Annex B). When this loading curve is followed to a chosen or real ultimate stress point and then unloaded, the elastic and “plastic” deformation is known of that limit point. (The “plastic” amount (permanent strain in Fig.D-1 depends on the past, unknown, loading history at growth, drying, manufacturing, transport and pre-testing).

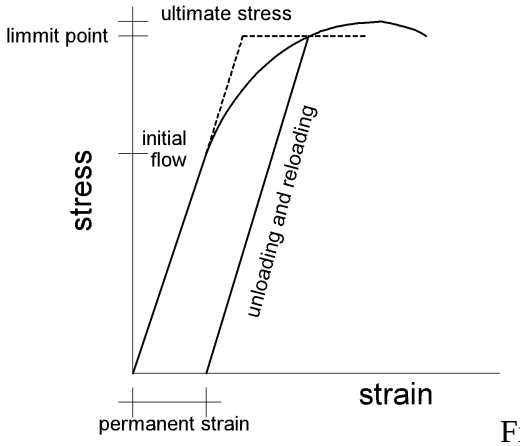

Fig.D-1. Loading curve

On reloading, the curve is elastic up to the limit point and it is possible to regard an elastic – full plastic description of the loading line according to the dashed line in Fig.D-1 as an allowable displacement field in the sense of limit analysis (that needs not to be the real occurring displacement for the virtual work equations). Also a reduced stiffness can be chosen as done for the Building Codes.

The virtual work equation, represents the extremum condition that the first variation of the potential energy is zero. Thus a small variation of the total potential energy vanishes when the structure is in equilibrium. Thus the total work of an equilibrium system is zero for any virtual displacement. The virtual work equation thus is based on an equilibrium set and a compatible set, which need not, and should not, be related. Thus:

$$\int_A T_i \dot{u}_i^* dA + \int_V F_i \dot{u}_i^* dV = \int_V \sigma_{ij} \dot{\varepsilon}_{ij}^* dV \,, \tag{D-1}$$

integrated over the whole area *A* and volume *V* of the body. T_i and F_i are external forces on surface and in the body; σ_{ij} are the stresses, in equilibrium with the external forces, which need not to be the real actual occurring stresses. The asterisk is used for the compatible set, to emphasize that the two sets are not related, thus are completely independent.

A valid equilibrium set must satisfy the equilibrium equations:

$$\frac{\partial \sigma_{ji}}{\partial x_j} + F_i = 0 \tag{D-2}$$

and the equilibrium conditions at the load applications points (as boundary condition).

Of the compatible set, are the strains $\dot{\varepsilon}_{ij}^*$ compatible with real or imagined (virtual) displacement rate $\dot{u}_i^*$ of the points of application of the external forces, following the strain and displacement rate compatibility equation.

$$2\dot{\varepsilon}_{ij}^* = \frac{\partial \dot{u}_i^*}{\partial x_j} + \frac{\partial \dot{u}_j^*}{\partial x_i} \tag{D-3}$$

Virtual displacements are not real, they can be physically impossible but they must be compatible with the geometry of the original structure and they must be small enough so that the original geometry is not significantly altered.

As equilibrium set, also the load increments can be used giving the rate equation:

$$\int_A \dot{T}_i \dot{u}_i^* dA + \int_V \dot{F}_i \dot{u}_i^* dV = \int_V \dot{\sigma}_{ij} \dot{\varepsilon}_{ij}^* dV \,. \tag{D-4}$$

In the linear-full plastic schematization is the plastic zone a line in Fig.D-2, but is a plane in

stress space. Plastic flow occurs when the yield function $f\left(\sigma_{ij}\right)=0$ is satisfied. It is necessary that:

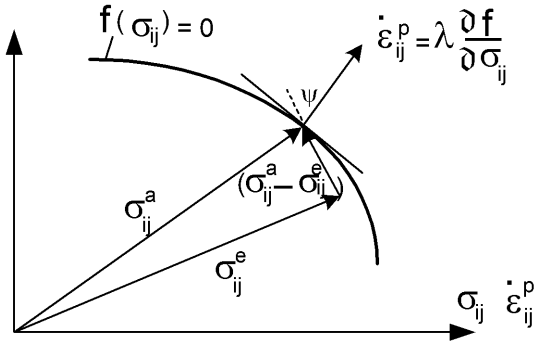

Fig.D-2 Yield surface and flow rule

$$\left(\sigma_{ij}^{a}-\sigma_{ij}^{c}\right)\cdot\dot{\varepsilon}_{ij}^{p}\geq 0\,, \tag{D-5}$$

Thus this dot product is always positive and shows an angle $\psi\leq 90^{0}$, because thermo-dynamical real work (and real dissipation) has to be positive. Eq.(D-5) only is for all cases fulfilled when the vector $\dot{\varepsilon}_{ij}^{p}$ is perpendicular to the curve $f\left(\sigma_{ij}\right)=0$, thus is in the direction of $\partial f/\partial\sigma_{ij}$. This is the convexity requirement or normality rule wherefore the principle of maximal local energy dissipation applies for the actual stress state, i.e. the projection in fig.D-2, of vector σ_{ij}^{a} on $\dot{\varepsilon}_{ij}^{p}$ is then maximal, higher than such projection of any other critical vector. In that case also the zero value of eq.(D-5) is reached for the plastic stress increment. Thus for the plastic flow increment then is:

$$\dot{\sigma}_{ij}\cdot\dot{\varepsilon}_{ij}^{p}=0 \tag{D-6}$$

From eq.(D-4) and (D-6) follows, that when the limit load is reached and the deformation proceeds under constant load, all stresses remain constant and only plastic, (not elastic) increments of strain occur. Because at collapse, eq.(D-4) becomes:

$$\int_{A}\dot{T}_{i}^{c}\dot{u}_{i}^{c}dA+\int_{V}\dot{F}_{i}^{c}\dot{u}_{i}^{c}dV=\int_{V}\dot{\sigma}_{ij}^{c}\dot{\varepsilon}_{ij}^{c}dV\,. \tag{D-7}$$

With $\dot{T}_{i}^{c}=\dot{F}_{i}^{c}=0$, and with elastic and plastic parts of strain, $\dot{\varepsilon}_{ij}^{c}=\dot{\varepsilon}_{ij}^{ec}+\dot{\varepsilon}_{ij}^{pc}$ is eq.(D-7):

$$\int_{V}\dot{\sigma}_{ij}^{c}\dot{\varepsilon}_{ij}^{c}dV=\int_{V}\dot{\sigma}_{ij}^{c}(\dot{\varepsilon}_{ij}^{ec}+\dot{\varepsilon}_{ij}^{pc})dV=\int_{V}\dot{\sigma}_{ij}^{c}(\dot{\varepsilon}_{ij}^{ec})dV=0 \tag{D-8}$$

because of eq.(D-6), and thus $\dot{\sigma}_{ij}^{c}\dot{\varepsilon}_{ij}^{ec}=0$. Thus the elastic strain increment and consequently, the elastic stress increment, are zero and all deformation is plastic. Thus the elastic characteristic plays no part in the collapse at the limit load.

Next it is possible to give the proof of the lower and upper bound theorems of limit analysis. The lower bound theorem states that, if an equilibrium distribution of stress σ_{ij}^{E}, covering the whole body, can be found, which balances the applied loads and is everywhere below yield $f\left(\sigma_{ij}^{E}\right)<0$, then the body will not collapse.

To prove this, assume that it is false, then two collapse equations exist:

$$\int_{A}T_{i}^{c}\dot{u}_{i}^{c}dA+\int_{V}F_{i}^{c}\dot{u}_{i}^{c}dV=\int_{V}\sigma_{ij}^{c}\dot{\varepsilon}_{ij}^{c}dV$$

$$\int_A T_i^c \dot{u}_i^c dA + \int_V F_i^c \dot{u}_i^c dV = \int_V \sigma_{ij}^E \dot{\varepsilon}_{ij}^c dV$$

and consequently is, because all deformation is plastic:

$$\int_V (\sigma_{ij}^c - \sigma_{ij}^E)\dot{\varepsilon}_{ij}^{pc} dV = 0, \qquad \text{(D-9)}$$

and because according to eq.(D-5): $(\sigma_{ij}^c - \sigma_{ij}^E)\dot{\varepsilon}_{ij}^{pc} > 0$ for σ_{ij}^E below yield, eq.(D-9) cannot be true and the lower bound theorem is proved.

The upper bound criterion states that if a compatible mechanism of plastic deformation is found, which satisfies the displacement boundary conditions, then the loads, determined by equating the rate, at which the external forces do work, eq.(D-10):

$$\int_A T_i \dot{u}_i^{p^*} dA + \int_V F_i \dot{u}_i^{p^*} dV, \qquad \text{(D-10)}$$

to the rate of internal dissipation, eq.(D-11):

$$\int_V D(\dot{\varepsilon}_{ij}^{p^*}) dV = \int_V \sigma_{ij}^p \dot{\varepsilon}_{ij}^{p^*} dV \qquad \text{(D-11)}$$

will be either higher or equal to the actual limit load.

Again, assume the theorem false, and the computed loads to be less than the actual limit load, then the following equation should apply:

$$\int_A T_i \dot{u}_i^{p^*} dA + \int_V F_i \dot{u}_i^{p^*} dV = \int_V \sigma_{ij}^E \dot{\varepsilon}_{ij}^{p^*} dV \qquad \text{(D-12)}$$

with σ_{ij}^E everywhere below yield. Because T_i and F_i follow from equating eq.(D-10) and eq.(11), it follows that:

$$\int_V (\sigma_{ij}^{p^*} - \sigma_{ij}^E)\dot{\varepsilon}_{ij}^{p^*} dV = 0 \qquad \text{(D-13)}$$

However, according to eq.(D-5) $(\sigma_{ij}^{p^*} - \sigma_{ij}^E)\dot{\varepsilon}_{ij}^{p^*} > 0$ for σ_{ij}^E below yield, what leads to a contradiction and thus to the proof of the upper bound theorem.

Some corollaries, to be mentioned, following from the lower bound theorem, are, that:

- Initial stress or deformation have no effect on the plastic limit or collapse load provided the geometry is essential unaltered. This is e.g. applied in **C(2014)**.
- The limit load, computed from a convex yield surface, which circumscribes the actual surface, will be an upper bound on the actual limit load. The limit load computed from an inscribed surface will be a lower bound of the actual collapse load. This last is applied in the derivations of e.g. **D(2008a)**, by using the, in the von Mises inscribed Tresca polynomial).

The graphical proof of the lower and upper bound is as follows:

In fig.D-3 is the plastic strain increment $\dot{\varepsilon}_c$ normal to the failure surface and is vector σ_l just inside the surface. Index *c* stands for actual collapse load and index *l* indicates lower bound.

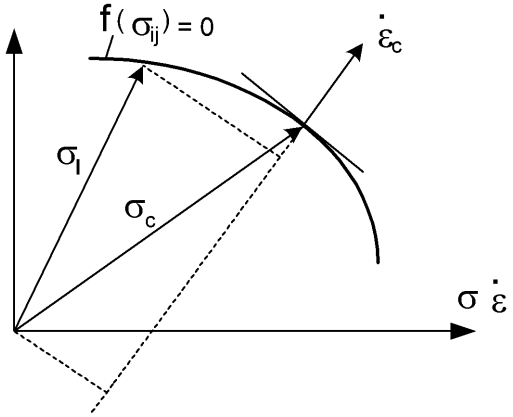

Fig.D-3. Proof of the lower bound theorem

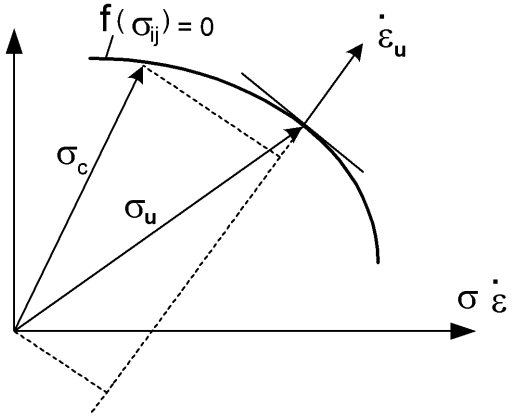

Fig.D-4. Proof of the upper bound theorem

According to the virtual work principle is for collapse:

$$\sum F_c \dot{w}_c = \int_V \sigma_c \dot{\varepsilon}_c dV$$

and for a lower bound:

$$\sum F_l \dot{w}_c = \int_V \sigma_l \dot{\varepsilon}_c dV$$

where *F* is the external force and *w* the displacement of *F*. The internal stress is σ_c with $\dot{\varepsilon}$ as strain increment. The dot product is the product of the strain increment with the components of the stress vector in the direction of strain increment. According to fig.D-3 is

$$\sigma_l \dot{\varepsilon}_c \le \sigma_c \dot{\varepsilon}_c$$

thus is a lower bound due to the convexity of the yield function.
For the proof of the upper bound criterion applies, according to fig.D-4, that collapse must have occurred if:

$$\sum F_u \dot{w}_u = \int_V \sigma_u \dot{\varepsilon}_u dV$$

According to the virtual work equation is: the upper bound criterion

$$\sum F_c \dot{w}_u = \int_V \sigma_c \dot{\varepsilon}_u dV$$

The figure shows by projection of σ_u and σ_c on $\dot{\varepsilon}_u$ that:

$\sigma_u \dot{\varepsilon}_u \geq \sigma_c \dot{\varepsilon}_u$

Thus also $F_u \geq F_c$ and F_u thus is the upper bound because of the convexity of the yield function.